Mechanisms of Dendrite Growth in Lithium Metal Batteries

Zur Erlangung des akademischen Grades
Doktor der Ingenieurwissenschaften
der Fakultät für Maschinenbau
Karlsruher Institut für Technologie (KIT)

genehmigte
Dissertation
von

Dipl.-Ing. Jens Steiger
aus Germersheim

Tag der mündlichen Prüfung:	15. Januar 2015
Hauptreferent:	Prof. Dr. rer. nat. Oliver Kraft
Korreferent:	Prof. Dr. rer. nat. Michael J. Hoffmann

Hiermit erkläre ich, dass ich die vorliegende Arbeit selbständig angefertigt und keine anderen als die angegebenen Quellen und Hilfsmittel benutzt sowie die wörtlich und inhaltlich übernommenen Stellen als solche kenntlich gemacht und die Satzung der Universität Karlsruhe (TH) zur Sicherung guter wissenschaftlicher Praxis in der jeweils gültigen Fassung beachtet habe. Hiermit weiße ich ausdrücklich darauf hin, dass Kapitel 5 und 6 bereits veröffentlicht wurden, siehe Literaturstellen [1] und [2]. Kapitel 8 ist zur Veröffentlichung angenommen, siehe [3].

Hiermit erkläre ich außerdem, dass für mich Promotionsverfahren außerhalb der Fakultät für Maschinenbau des Karlsruher Instituts für Technologie (KIT) weder anhängig sind noch erfolglos abgeschlossen wurden.

Acknowledgements

Die vorliegende Arbeit entstand während meiner Zeit als Doktorand am Karlsruher Institut für Technologie (KIT) am Institut für Angewandte Materialien (IAM) in der Abteilung für Werkstoff- und Biomechanik (WBM). Im Folgenden möchte ich mich bei den Personen bedanken, die maßgeblich zum Gelingen dieser Arbeit beigetragen haben.

Prof. Dr. Oliver Kraft danke ich für die Aufnahme an seinem Institut und für die Betreuung und Unterstützung dieser Arbeit.

Prof. Dr. Michael J. Hoffmann danke ich für die Übernahme des Korreferats.

Meinem Betreuer Dr. Reiner Mönig möchte ich für die freundschaftliche und produktive Zusammenarbeit danken. Seine wissenschaftliche sowie experimentelle Unterstützung war essentiell für das Gelingen dieser Arbeit. Im gleichen Maß bin ich Dr. Dominik Kramer zu Dank verpflichtet. Ich hätte mir keine bessere Arbeitsgruppe wünschen können.

Allen Kollegen am IAM-WBM möchte ich für die fantastische Zeit, die Hilfsbereitschaft und die wissenschaftlichen Diskussionen danken. Ganz besonders bedanken möchte ich mich bei Moritz Wenk, Grant Boggess, Dr. Steven Boles, Dr. Di Chen und Dr. Zungsun Choi.

Meiner Familie, ganz besonders meinen Eltern Gabi und Bernhard, danke ich von ganzem Herzen für die liebevolle Unterstützung auf meinem bisherigen Weg. Außerdem möchte ich meinem Patenonkel Dr. Karl-Josef Dickerhof an dieser Stelle noch einmal besonders für seine Unterstützung danken.

Meiner Freundin Bianca möchte für die Liebe und den Rückhalt auf unserem gemeinsamen Weg danken; und dafür dass sie mir immer den Rücken frei gehalten hat.

Kurzfassung

Das Wachstum von Lithiumdendriten in wiederaufladbaren Batterien verursacht nicht nur einen starken Kapazitätsverlust, sondern stellt wegen der Möglichkeit eines Kurzschlusses auch ein beträchtliches Sicherheitsrisiko dar. Hauptsächlich betroffen von diesem Problem sind Lithiummetall enthaltende, wiederaufladbare Batterien; es können aber auch Lithium-Ionen-Systeme betroffen sein, obwohl diese ursprünglich entwickelt wurden, um die Dendritenproblematik zu umgehen. Dieses Phänomen ist nun schon seit mehr als 50 Jahren bekannt, dennoch konnten die in der Literatur vorgeschlagenen Lösungen weder das Sicherheitsproblem noch das Problem der geringen Kapazität gleichzeitig lösen. Trotz der umfangreichen Grundlagenforschung zu Dendriten sind die zugrunde liegenden Mechanismen immer noch nicht eindeutig geklärt. In der vorliegenden Arbeit werden optische *in-situ*-Untersuchungen durchgeführt, um neue Einsichten in die elektrochemische Abscheidung von Lithium zu gewinnen. Mit Hilfe der Daten aus diesen Experimenten und zusätzlichen REM-Untersuchungen konnten Mechanismen des Dendritenwachstums auf verschiedenen Größenskalen identifiziert werden. Es stellte sich heraus, dass Nadeln das Frühstadium des verzweigten Wachstums sind. Diese Lithiumnadeln entstehen auf verschiedensten Substraten und sogar während der Abscheidung aus der Gasphase, sodass die Elektrochemie als beherrschender Einflussfaktor in diesem Stadium ausgeschlossen werden kann. Nadeln wachsen während der elektrochemischen Abscheidung durch Insertion von Lithiumatomen an kristallinen Defekten, d.h. an der Basis, an der Spitze und an Knicken der wachsenden Struktur. Sobald sich diese Insertionsdefekte vervielfachen und gleichzeitig aktiv werden, verzweigt sich die Nadel und geht in einen Busch über. In dieser Doktorarbeit werden detaillierte Beobachtung der Entstehungs- und Wachstumsmechanismen poröser

Lithiumabscheidungen beschrieben. Es werden außerdem zusätzliche Aspekte wie z.B. die Reversibilität (Abscheidung und Wiederauflösung) und der Einfluss des Elektrolyten auf das Wachstum der Lithiumstrukturen behandelt. Die vorgestellten Ergebnisse könnten sich bei der Entwicklung von Strategien zur Vermeidung des Dendritenwachstums als nützlich erweisen. Das ist ein zentraler Punkt für die Lithium-Ionen-Systeme heutiger Bauart und für die Umsetzung zukünftiger Batteriekonzepte wie Li-S und Li-O.

Abstract

Lithium dendrite growth in rechargeable batteries not only causes strong capacity fading and a limited lifetime, it also causes severe safety concerns as dendrites can short-circuit the cell. Dendrites primarily affect lithium metal based rechargeable batteries, but also to some extent today's lithium-ion systems that were introduced to circumvent this problem. Although this phenomenon is known for more than 50 years, none of the presented remedies are able to sustainably tackle both the safety issue as well as the low cycling performance. Despite the extensive research that has been performed on the fundamentals of dendrite growth, the underlying mechanisms are still not clear. In this work *in situ* light microscopy with unmatched spatial resolution was performed in order to obtain insights into lithium deposition. Data from these experiments together with SEM observations helped to identify mechanisms associated with lithium dendrites at different length scales. It was found that the early stages of the ramified structures are filaments. These lithium needles can form on various substrates even during physical vapor deposition so that electrochemistry can be excluded as a governing factor at this stage. The needles then grow by a lithium insertion mechanism where during electrodeposition lithium is inserted at crystalline defects such as the interface at the base, at kinks, as well as at the tip of the growing structures. Once insertion defects multiply and simultaneously become active, branching occurs and the needle transitions into a bush. This thesis deals with the detailed observation and description of the mechanisms controlling formation and growth of irregularly shaped lithium deposits. It addresses aspects such as the effect of the electrolyte on the growth as well as the reversibility (deposition-dissolution) of the lithium struc-

tures. The presented results may become useful in finding strategies for preventing lithium dendrites, which is a key issue for current lithium-ion batteries but also future lithium metal based battery concepts such as Li-S and Li-O.

Contents

1 Introduction

High levels of air pollution in cities and industrial areas as well as the rising awareness for environmental damage and climate change has given rise to a growing demand for emission free and environmentally friendly energy storage and conversion systems. The applications range from stationary storage systems for load-leveling of solar cells and wind turbines to storage systems for electric or hybrid mobility. In addition to reducing emissions, another challenge for storage systems is the energy thirst of today's portable electronic devices; currently, these systems already represent over one third of the overall product weight. Promising candidate technologies for these challenges are battery systems. So far, lithium-ion batteries have taken the lead role in electric cars as well as in laptops and smartphones. Fig. 1.1 shows a Ragone plot for different battery technologies, showing the superior performance of state-of-the-art lithium-ion systems (blue) in terms of weight and size(featuring cathode materials like lithium iron phosphate, manganese oxides and cobalt oxide) when compared to lead-acid or nickel-metal-hydride cells. These advantages have made lithium-ion batteries the market leader for mobile applications. Also for stationary applications, lithium-ion batteries are of very high interest due to their high cycle life as compared to the widespread lead-acid batteries.

In lithium-ion batteries, independent of their cathode materials depicted in **Fig. 1.1**, carbon-based anodes are commonly used. Pairing lithium metal instead of carbon-based anodes with current electrodes offers an improved specific energy (gravimetric) and an even more strongly improved energy density (volumetric) as indicated in Fig. 1. This is caused by the tremendous difference in theoretical capacity between pure lithium metal (3860 mAh g^{-1}) and the carbon anodes used today (372 mAh g^{-1}).[4] In addition,

lithium metal offers the lowest negative electrochemical potential of all elements with −3.040 V vs. a standard hydrogen electrode.[5] These facts make lithium metal the anode of choice and has led to wide spread use of lithium metal as anodes in primary (i.e. non-rechargeable) cells since their first commercialization in 1973 by Panasonic [6].

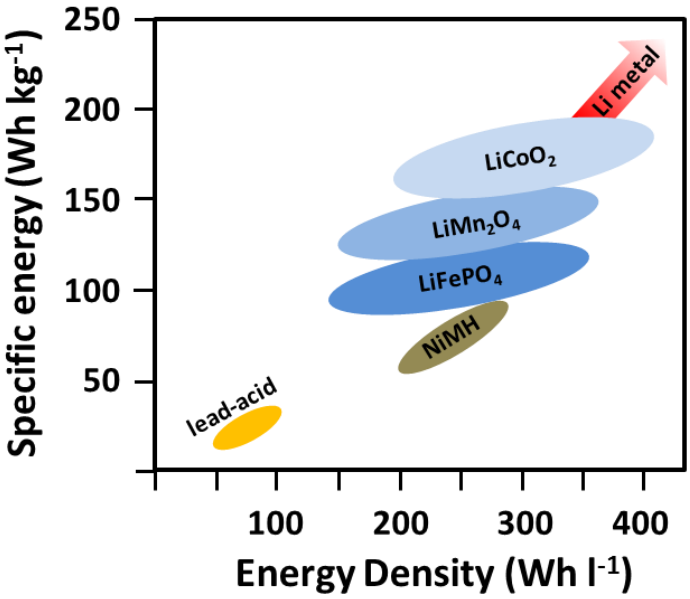

Fig. 1.1: Ragone plot: The specific energy (Wh kg^{-1}) of different battery technologies plotted over their energy density (Wh l^{-1}).[7-9]

Unfortunately, lithium metal anodes show strong disadvantages when it comes to recharging the cell. They suffer from low Coulombic efficiency, low cycling performance as well as the danger of short-circuiting and subsequent thermal runaway. These drawbacks are mainly caused by the so-called dendritic deposition of lithium metal. During charging, lithium does not

form a flat, homogeneous layer on the anode, but instead creates various ramified structures generally referred to as dendrites that can be needle-like or branched. Due to this issue, lithium metal anodes in secondary (i.e. rechargeable) batteries have not seen wide-spread application – in contrast to lithium primary cells. Nonetheless, a lithium metal / MoS_2 rechargeable battery was commercialized in the late 1980s by Moli Energy. It had a three-fold excess of lithium to compensate for the low cycling performance that causes continuous capacity loss during cycling. In 1989 however, they were recalled due to safety issues as several of these battery systems vented under spurts of flame due to internal overpressure, probably caused by thermal runaway [10].

It was not until the early 1990s that Sony commercialized the first lithium-ion battery and replaced the lithium metal anodes by graphite – in principle the same type of anodes that are still used in today's lithium-ion cells. With the graphite anode, Sony was able to circumvent the problem of lithium deposition, but sacrificed the more electronegative potential of pure lithium (~0.2..0.1 V [11]) and the higher specific energy. Unfortunately, the problem of dendritic deposition of lithium can still be a problem in today's systems, as the intercalation process into the graphite can be too slow under certain conditions, which causes the lithium to be deposited in its metallic form onto the graphite surface. These conditions can be a low operating temperature which slows down the intercalation process, or a charge rate that is too high. An extreme case is the overcharging of the cell where the capacity of the cathode is in excess compared to the anode (bad capacity balancing or disconnections of parts of the anode). Under these conditions the graphite electrode cannot accommodate all of the lithium and plating will occur.

Numerous product recalls of rechargeable lithium-ion batteries have taken place within the last years, the most prominent

being the recall of Sony laptop batteries in 2006: An estimated 7 million devices worldwide were called back to the factory by different laptop manufacturers, amongst them over four million recalled by Dell and 1.8 million by Apple. The most recent recall started in April 2014, when Sony called back Vaio Fit 11A laptops featuring a Panasonic battery pack. Although the origin of the overheating or fires in these batteries is usually kept a manufacturer secret, researchers have speculated that dendrites have caused the short circuits [12]. These shorts lead to rapid discharge and overheating. The most prominent case of lithium-ion battery problems were the series of fires that broke out on-board the Boeing 787 planes while being in mid-flight. This resulted in the grounding of the entire Boeing 787 in early 2013; dendrite formation quickly came under suspicion and has been under investigation by aviation safety investigators [13].

"Next generation" rechargeable battery systems that are currently under investigation are attempting to increase the energy and power per volume and per mass to reach values closer to current internal combustion (IC) based systems. These future systems include lithium-sulfur and lithium-oxygen cells. While lithium-oxygen has the theoretical potential to approach the specific energy of the gasoline tank of the IC system, lithium-sulfur is closer to commercialization[14]. However, for highest energy densities, both systems require a lithium metal anode and therefore will most likely also be affected by dendritic deposition.

Even after over 50 years of research on this topic no technologically viable solution to safely apply lithium metal anodes in secondary cells has been established and the shear amount of publications on this topic underline the unbroken research interest. To date, the mechanisms underlying dendritic lithium deposition are still not clear. Several properties of lithium and lithium based cells make research on this topic very challenging: Lithium

has atomic number 3 and is the least dense solid element and therefore a weak scatterer for electrons and x-rays. This makes the determination of the crystal structure and orientation challenging. Lithium is highly reactive even under nitrogen. Common liquid battery electrolytes are volatile and opaque for electrons and prevent *in situ* studies of liquid systems e.g. by electron microscopy. As a result, even basic questions such as where a dendrite grows – by adding atoms to the tip, to the base or somewhere else – is still under debate today.

2 Background

2.1 Introduction to Lithium-ion Batteries

The word battery is usually used to refer to – what is technically – an array of electrochemical cells. An electrochemical cell basically consists of two electrodes immersed into an electrolyte. These electrodes are made of an electrochemically active material and a current collector. The principle of a battery exploits the electrochemical potential difference between the active materials. In order to create a high cell voltage, the active materials should be selected accordingly as the potential difference gives the voltage of the cell. The negative electrode is referred to as the anode, the positive electrode as the cathode.[1] The electrolyte acts as an electronic insulator and ionic conductor. A separator – mostly porous, ceramic- or polymer based and soaked by electrolyte – is placed between both electrodes to avoid the contact between the electrodes that would result in an electrical short-circuit.

In a lithium-ion battery, graphite is commonly used as an anode material and a transition-metal oxide or phosphate is used as a cathode material (see **Fig. 2.1**). The electrodes are typically manufactured by forming slurries of active material powder, binder and a solvent. A conductive powder – often carbon black – is used to compensate for the rather poor electronic conductivity of the metal oxide cathode materials. In most cases the slurry is coated onto aluminum foil in the case of cathodes or on a copper foil in the case of anodes; these foils act both as mechanical sup-

[1] However, this denotation is only correct during discharge as the chemical processes at the electrodes are reversed during charging. In the field of battery research, the negative and the positive electrode are always called anode and cathode respectively regardless of charging or discharging in order to avoid confusion.

port and as current collectors. After evaporation of the solvent, a porous film typically in the range of 50 to 200 µm remains. A certain degree of porosity in the film is desirable as it increases the interface area with the electrolyte. Porous electrodes have shorter solid state diffusion paths and with the help of the carbon black also better electronic conductivities.

Both anode and cathode materials allow for the lithium ions to intercalate into their crystal structure, as sketched in Fig. 2.1. This means that the ions are reversibly inserted into the host structure of the active material without strongly altering the crystal structure of the host. In the charged state, the lithium atoms are stored in between the individual layers of the graphite. During discharge, the lithium atoms are deintercalated and dissolved at the anode. At the cathode, the lithium cations are inserted into the crystal structure of the positive active material; in commercial systems this can be for example a layered structure (e.g. $LiCoO_2$), a spinel structure (e.g. $LiMn_2O_4$) or an olivine structure (e.g. $LiFePO_4$). To compensate for the charge that is transported by the ion, an electron flows from the anode through the electrical wiring to the cathode. Inside the cathode, the lithium cation diffuses into an empty lattice site. There, also an electron arrives which is transferred to the transition metal so that the transition metal gets reduced. The electrolyte transports the positively charged ions (Li^+) while the negative charged electrons (e^-) are carried by the wiring. The electron current together with the cell voltage delivers the electrical power. During charge, the processes are reversed (transition metal is oxidized) and the cell acts as a sink so that energy is stored. The electrolyte is often not chemically stable against the electrode; hence a layer consisting of decomposition products of the electrolyte and the electrode forms on the electrodes. This layer, the so called solid electrolyte interface (SEI) (see **Fig. 2.1**) is penetrable for lithium cations and can protect the electrodes and the electrolyte against further degradation.

In order to intercalate lithium into graphite, six carbon atoms are needed to accommodate one lithium atom. As a result, graphite cannot reach the energy density and specific energy of a lithium metal anode. Here, lithium metal can be directly electrodeposited onto the anode and no additional material is needed to accommodate it or to increase its electric conductivity. However, the capacity of today's cathodes is still –by a factor of two –smaller than that of graphite anodes, which makes the cathode the bottle neck for lighter battery designs. Nevertheless, strong improvements can be achieved in terms of volume by using silicon or lithium metal anodes. The smaller volume of the lithium anode also allows for smaller volumes of the electrochemically inactive components so that increases in volumetric energy densities at the cell level of more than 200 % are possible.[15] Unfortunately, both silicon and even more so lithium are not yet ready for commercialization.

2.2 Growth of Dendrites and Related Structures

As the cause and the mechanisms of dendritic growth are still under debate, various theories and explanations were presented in the past. An overview is given in the following section including experimental results as well as theories of ramified or needle-like growth that have their origin outside of electrochemistry. The needle-like growth will be often referred to as one-dimensional growth in the following, while the ramified, branched growth will be often referred to as three-dimensional.

The term dendrite, derived from the Greek word for tree (δένδρον *déndron*), describes a multi-branched structure and is a common form of solidification of metals, e.g. from the molten state or during electrodeposition. Dendrite formation during electrodeposition was reported for various metals, e.g. silver [16] copper

[17] and zinc [17], 3D growth of tree-, bush-, moss- and even needle-like dendrites was found. However, these mechanisms have been verified usually based on aqueous electrolyte systems where no SEI formation is expected, so their applicability for lithium in nonaqueous systems needs to be verified. Various alternative theories have been developed to explain dendritic growth. The ones relevant for this work will be presented in the following.

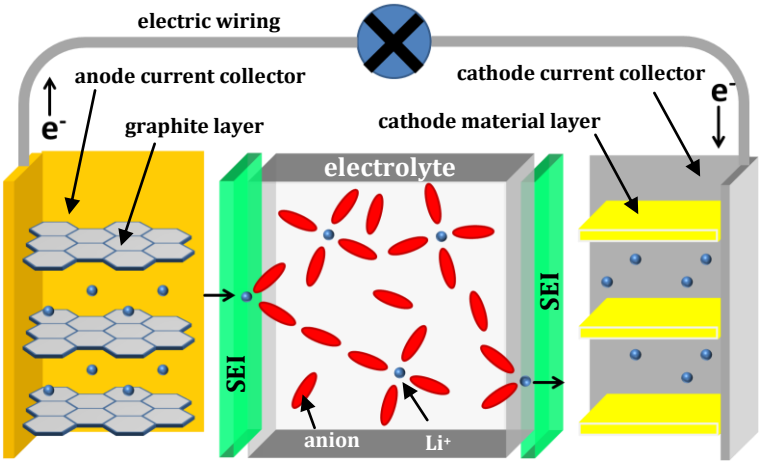

Fig. 2.1: Schematic of lithium-ion cell working principle. In the charged state, lithium is stored in between the graphite layers; during discharge, the lithium cation travels through the electrolyte to the cathode, while the electron travels through the electric wiring creating the electrical current that the cell delivers. At the cathode, the lithium atom is placed inside the crystal structure of the cathode material. The SEI is ion-conductive and prevents further degradation.

2.2.1 Ionic Concentration Gradient in the Electrolyte

An important factor can be the ionic concentration gradient in the electrolyte. During deposition, the concentration of metal cations will drop at the negative electrode where these ions are removed from the electrolyte, while their concentration will rise above the initial value close to the positive electrode where metal cations enter the electrolyte. The limiting current density J^* marks the current density an electrochemical system is able to sustain – theoretically – for unlimited time. In batteries, there is no stirring and no convection (since this is blocked by the porous separator), which means that the concentration gradient spans the whole electrode distance L. In this case and for a monovalent ion, J^* is given by

$$J^* = \frac{2\, e\, C_0\, D}{t_a\, L} \tag{1}$$

with e being the elementary charge, $C_0$the initial ion concentration in the electrolyte, D the diffusion coefficient and t_a the anionic transference number.[5] This means that especially in dilute solutions or solutions with a low diffusion coefficient, the limiting current is smaller. When the limiting current is exceeded, the cell will supply this current only for a limited time. This time is called Sand's time τ and it marks the time when the ionic concentration at the electrode drops to zero. It is given by

$$\tau = \pi\, D \left(\frac{e\, C_0}{2\, J\, t_a}\right)^2 \tag{2}$$

After this time, the potential diverges since no charge carriers are available anymore. Despic and Popov [18] identified the influence of a complete concentration polarization on the ramification of the electroplated species. On this basis, Fleury et al. [19] and Chazalviel [20] established their own mathematical growth

model considering a binary electrolyte and found that once the ionic concentration has dropped to zero, the condition of electroneutrality in the electrolyte is violated at the negative electrode. This supposedly leads to local space charge, and as results ramified structures are expected to form. These structures are predicted to grow at the speed of the anion drift velocity in the electrolyte, which is given by

$$v_a = \mu_a E_0 \tag{3}$$

with μ_a being the anion mobility and E_0 being the local electric field. They are expected to form after Sand's time. Brissot et al. [21] experimentally confirmed ramified structure growth at anion drift velocity in a lithium/PEO-LiTFSI/lithium cell and later they also observed that the electrolyte in the vicinity around dendrites was depleted of ions [22]. This model falls short in predicting the onset of dendritic growth under low current density conditions. Under these conditions, no Sand's behavior is expected as the concentration gradient in the electrolyte is not steep enough; so according to the model, no dendrites are expected to form. However, Rosso et al. [23] found dendrites to form under these conditions in a lithium/polymer/lithium cell. They attributed this to the existence of surface inhomogeneities on the lithium which they ascribed to specific properties of the PEO-LiTFSI polymer electrolyte. This way, fluctuations in the local current density can occur so that the ionic concentration at the electrode can drop to zero locally.

According to equation (2) the current density J is an important influence factor. Rosso et al. [24] could show experimentally that the short-circuiting through dendrite growth in a lithium polymer cell appeared faster with increasing current density. They stated that the time until a short happens roughly scales with J^{-2}. According to Crowther and West [25], the initiation time of dendritic growth scales with J^{-1}. Orsini et al. [26, 27] found that with in-

creasing current density, the morphology of the deposited lithium changed from moss-like to tree-like (they referred to it as dendritic) in a lithium polymer cell. Similarly, Dollé et al. [28] found that morphology changed from moss-like to needle-like with increasing current density. In contrast to that, Brissot et al. [21] observed a change from needle-like to bush-like dendrites with increasing current density using the same polymer electrolyte.

A moving, dynamic electrolyte should be able to relax the concentration gradient that can form in a stagnant electrolyte and should hence be able to reduce the tendency to grow dendrites. Accordingly, it could be shown that an impinging flow of electrolyte could suppress the formation of dendrites during zinc electrodeposition in contrast to a stagnant electrolyte under the same working conditions.[29] The influence of a moving 1 M $LiPF_6$ in EC/DMC electrolyte by using a magnetic stirrer was also investigated. At a current density of 2 mA cm^{-2} smooth, hemispherical plating of lithium was observed, while static conditions gave dendritic deposition, even at 0.5 mA cm^{-2}. An improved cycling efficiency when compared to a stagnant electrolyte was also reported.[30] Crowther and West [25] observed a delayed dendrite initiation time in their microfluidic setup with the electrolyte flowing in plane with the electrode surface. This effect was not depending on the electrolyte that was used. They also reported that dendrites in a stagnant electrolyte would branch more quickly and more often.

Based on a simulation with a coarse-grained lattice model, it was suggested that pulse charging could be applied to the electrodeposition of lithium metal as an attempt to suppress dendrite formation.[31] It was argued that dendrite formation is the product of a competition between lithium-ion diffusion in the electrolyte and the reduction process on the electrode. According to the model, the pause between two pulses can successfully shift this

competition in favor of the ion diffusion. Thus, it can reduce the overpotential at dendrite branches as it relaxes the ionic concentration depletion that has formed there.

Solvent in salt

A new class of electrolytes for the application in lithium sulfur cells that was reported to suppress dendritic growth and to improve the cycling efficiency was created by Suo.et al.[32] This new class was a solvent-in-salt electrolyte that provided an ultrahigh salt content up to 7 mol/l and high lithium-ion transference number. They further showed that lithium polysulfide dissolution is inhibited, which means they were able to overcome the 'polysulfide shuttle phenomenon'. However, it was remarked that "too high a salt concentration will lead to increased cost and weight so an optimized salt concentration needs to be identified for practical applications [5]".

2.2.2 SEI Non-uniformity

The SEI can reach thicknesses of up to several tens of nanometers depending on current density, electrolyte and the electrode [33], has a "non-negligible" mechanical strength and a complex, inhomogeneous composition. Hence, it might not be appropriate to call this layer an inter*face*, as an inter*face* is only two-dimensional by definition. The word inter*phase* appears to be more suited as it better represents the three-dimensionality of the SEI and its properties. Basically two views about the morphology of the SEI exist in the literature.[34] Some authors describe it as a two layer system, with the lower layer closest to the substrate being crystalline, dense and mostly comprised of lithium salts. The upper layer is described as rather soft, porous and dominated by polymeric content.[35] Other authors describe the SEI as "a mosaic-type, multilayered structure" [36] formed by the simultaneous reduc-

tion of the salt (forming the crystalline salt precipitates) and the solvent (forming the polymeric components) without a distinct separation between the upper and lower layer.

Based on the latter theory, Cohen et al. proposed [36] a dendrite growth model based on the inhomogeneous nature of SEI. They argue that in a nonaqueous solution, the SEI is intrinsically non-uniform on the nanometer and even on the micrometer scale. This causes localized deposition and stripping at parts of the SEI that have a higher ion-conductivity, either due to a smaller thickness or due to more ion-conductive composition. This results in a stress between the shape changing lithium layer and the SEI on top. For high current densities, the SEI might not be able to withstand the induced stress and cracks, which exposes an area of the lithium without SEI, thereby increasing the localization even further. During stripping, the inhomogeneous current distribution causes deep pits in the lithium, and for plating this can be the cause for dendritic growth.

Accordingly, adequate SEI design could help to prevent dendritic growth. The electrolyte strongly influences the SEI composition of an electrode, as the SEI mainly consists of the decomposition products of the lithium, the solvent and the Li salts of the electrolyte. Consequently, the influence of different salts, solvents and additives has been studied.

Salts

The composition of areas of the SEI that are closer to the substrate is dominated by the decomposition products of the anions of the Li salts. These products are mainly inorganic salts. It is assumed that if these salts form a strong and homogeneous layer, they might be able to suppress dendritic growth.[5] Aurbach and Cohen [37] used AFM and compared the influence of $LiClO_4$ and $LiPF_6$ salts on the morphology of Li electrodeposited onto a Cu

substrate. They found that $LiPF_6$ created a more uniform deposition. They attributed this to the more homogeneous nature of the SEI formed in $LiPF_6$. While $LiClO_4$ creates a surface film that mainly consists of $ROCO_2Li$ (R is an organic group depending on the solvent), Li_2CO_2, Li halides and $LiOH\text{-}Li_2O$, the surface film in $LiPF_6$ mainly consists of LiF.[38] They later compared the performance of both salts with $LiAsF_6$ salt in a PC solution and found that $LiAsF_6$ creates even smoother surfaces and consequently lead to a higher cycling efficiency.[39] A newly developed $LiN(C_2F_5SO_2)_2$ (LiBETI) salt was reported to be superior in terms of cycling efficiency and cycle life in comparison to – amongst others – $LiPF_6$ salt in a PC solution. It was stated that the LiBETI salt formed a surface film that consisted mainly of LiF similar to $LiPF_6$ and also gave a similarly smooth and hemispherical Li layer.[40]

Solvent

A wide range of organic solvents has been investigated. It was found that – in combination with $LiClO_4$, $LiPF_6$, $LiAsF_4$ and $LiBF_4$ lithium salts – only the two ethers DME and DEE and the four esters PC, EC, DMC and DEC offer an oxidation potential in a Li metal battery with a $LiMn_{1.9}Co_{0.1}O_4$ cathode which is high enough.[41] Amongst all possible combinations of solvent and salts, an even mixture of EC and DMC showed the highest cycling performance using 1 mol/l $LiPF_6$.[41] Crowther and West showed that the initiation of dendritic growth could be delayed with a lower PC content in a PC/DMC based electrolyte using lithium bis(trifluoromethane sulfonyl) imide (LiTFSI) as salt.[25] Xu et al. listed the average Coulombic efficiency of several solvents reported in the literature.[5] Even though many of the tested solvents reach values well above 95 % Coulombic efficiency, they show weak cycling performance and fail to prevent internal short circuits caused by dendritic growth. 1,3-dioxolane (DOL) in com-

bination with $LiClO_4$ however, as reported by Aurbach et al. [42], shows an outstanding cycling performance and was found to successfully suppress dendritic deposition of lithium. This was attributed to the high elastomeric content in the SEI, which makes it flexible enough to withstand the volume changes in the lithium electrode during cycling without cracking, in contrast to other SEI layers formed in different solvents.[43]

Additives

Large efforts were put into the search for electrolyte additives suppressing dendrites, as the selection of solvents and salts is comparably small. Amongst many, HF was intensively investigated [5]. Similar to the fluoride containing salts like $LiPF_6$, HF enhances the formation of a homogeneous distribution of LiF and LiO_2 on the lithium surface which leads to smooth and hemispherical deposition of lithium. However, this protective effect wears off after several cycles, as the SEI is eventually too thick for HF to reach the electrode surface.[44, 45]

Although vinylene carbonate (VC) was reported to decrease the cycling efficiency in combination with $LiClO_4$ salt and PC solvent [46], it improved the cycling efficiency at ambient and higher temperature in EC/DMC based electrolytes independent of the salt used [47]. However, this study also showed that VC worsened the cycling efficiency and lead to a thicker surface film at 0 °C.

Metal ions such as Sn^{4+}, Sn^{2+},Al^{3+}, In^{3+},Ga^{3+} and Bi^{3+} with a higher reduction potential than Li were also found to improve the Coulombic efficiency and suppress dendritic growth.[48-50] These metal ions are reduced on Li and are expected to alloy with it, forming a thin alloy layer on the lithium electrode, preferentially at active points of the surface were dendrite would have formed otherwise. The co-deposition of Mg [51], Na [52] or K [53] was

also observed to improve the deposition quality. They do not alloy with lithium, but are expected to deposit on specific crystal faces of the lithium that are especially active and could lead to dendrite formation.

2.2.3 Spherical Diffusion

Barton and Bockris [16] studied the growth of silver dendrites in a solution of $AgNO_3$ in an equimolar mixture of molten $NaNO_3$ and KNO_3. They proposed a model for dendrite growth below the limiting current based on the fact that deposition from a liquid electrolyte will be faster on thinner and elevated parts of the surface as they will benefit from a spherical diffusion. While on ideally flat surfaces linear diffusion conditions will dominate, a 3D diffusion will be dominant for protrusions. For a spherical diffusion (spherical symmetry), the highest current densities and fastest growth occur at the dendrite tips with the smallest radius. Since experimental results report a round or flat tip with a rather constant diameter of the dendrite, they introduced the surface energy to counteract the tendency towards infinite narrowing of the tip and to limit the growth rate. The growth speed v of a dendrite growing at its tip is

$$v = J_n V_M / z\, F \tag{4}$$

with J_n being the local current density at the tip, V_M being the molar volume of the dendrites, z is the valence and F the Faraday constant. They also predicted the existence of a tip radius at which the growth speed is maximal.

Monroe and Newman [54] and Akolkar [55] expanded the model of Barton and Bockris to allow for changing ionic concentration in the electrolyte. Monroe and Newman's one-dimensional model of a single isolated needle predicts that a dendrite accelerates with time and traversed distance. It is also predicted to grow

faster for higher current densities, and can be slowed down by reducing the current during the plating process. They used the simplification that the tip is hemispherical and static.

2.2.4 Edge Effect in Electric Fields

It is well-known that the charge carriers in an electrically charged volume will not distribute evenly across the volume, but will show a higher charge density close to the surface of the volume. The charge density will become even higher at protrusions. This was suggested to lead to a stronger electric field at these protrusions. In the case of protrusion on a charged electrode surface inside an electrochemical cell, it is argued that it is the locally enhanced electric field is what is causing dendrite growth by preferred plating at the tip of the protrusion rather than on the substrate surface.[56, 57] This effect is expected to be self-enhancing, as plating at a protrusions tip further increases the protrusions length, and hence increasing the local electric field. [57]

Based on this dendrite growth theory, Ding et al. have suggested a dendrite suppression mechanism, called self-healing electrostatic shield (SHES).[57, 58] According to them, metal ions like Cs^+ can be added to the electrolyte in such a low concentration that their reduction potential remains below the reduction potential of Li^+. So instead of depositing, the Cs^+ cations are expected to be adsorbed at the electrode surface as they are attracted by electrostatic forces; this creates a layer of cations that repels the also positively charged lithium cations. Due to the edge effect in electric fields, the electrostatic force is higher at protrusions than at recessions or flat surfaces. This is then expected to cause accumulation of the foreign metal cations at these protrusions, which actively shields further deposition of lithium at protrusions – particularly at dendrites and directs the plating towards recessed and flat areas. In an experiment, a smooth lithium deposit was

obtained in 1 M $LiPF_6$ in PC with $CsPF_6$ concentrations of 0.01 and 0.05 M.[57, 58] A closer inspection of the supplied SEM images still shows the evolution of roughness. The achieved Coulombic efficiency is very low due to the PC-based electrolyte, and due to the narrow potential window between the reduction of Cs^+ and Li^+, the current density must be kept low.[58]

2.2.5 Statistical Roughness Evolution

Even though the kinetic roughening – a common effect in statistical mechanics [59]– cannot be responsible alone for dendritic growth, it can still be a trigger for dendritic growth by statistically creating protrusions on an electrode surface. Several theories were proposed that rely on the existence of initial surface protrusions, e.g. ionic concentration gradient in the electrolyte or the edge effect in electric fields, which could be provided by this effect. Kinetic surface roughening during chemical vapor deposition follows statistic rules; and hence surface roughness increases with increasing deposition thickness until the surface roughness reaches a steady state. Cuerno et al. have shown that their simulation results of kinetic roughening for chemical vapor deposition can also be applied to galvanostatic electrodeposition.[60, 61]

2.2.6 Whisker-like Growth

A model that considers the onset of dendritic growth as whisker growth process was put forward by Yamaki et al. [62] based on the observations made in an electrolyte of $LiAsF_6$ in EC/2MeTHF. They suggested that lithium dendrites grow from the base, and after a while they saw deposition of lithium at the tips and kinks of dendrites. They believe that lithium ions get plated non-uniformly underneath the SEI due to locally higher ionic conductivities. This creates a stress between the SEI and the underlying lithium substrate. The lithium metal reliefs the stress by atom

transport, but this transport is conditioned by the surface tension of the curved lithium surface and the SEI. Eventually the SEI cracks open and the lithium metal is then able to relief the stress by extruding trough the crack. This causes the formation of needle-like lithium. They stated that this process is similar to tin whisker formation due to compressive stresses, and that the formation of kinks of the needles is also known for whiskers. Once the electrode surface is densely covered by lithium needles, ionic transport to the surface is hindered, and lithium is plated directly onto the needle, preferably at the kinks or tips. In this process the morphology changes to – what they call – a mushroom-like shape.[63] Their mathematical model predicts that if the creep strength of the whisker is smaller than the pressure caused by the surface tension, the needle will become instable. This would make it desirable to increase the surface tension to create particle-like deposits instead of needles.[62]

2.2.7 Other Countermeasures

The aforementioned influence factors deal with electric fields, diffusion inhomogeneities or electrolyte/SEI aspects, i.e. they are tackling the dendrite problem directly by targeting underlying mechanisms. Nevertheless further research has been performed on how lithium plating can be influenced indirectly. A selection of this literature is summarized below.

Increased Shear Strength: Gel, Solid Electrolytes

Mechanical means of dendrite suppression have been studied. These means reach from increasing the shear modulus of the liquid electrolyte over the usage of dense separators to the application of solid electrolytes. Fumed silica added to the electrolyte was reported to form a continuous network that is able to restrict dendrite growth and to scavenge impurities from the electrolyte.[64] The same mechanical suppression effect was reported for

gel-type electrolytes.[65] Solid polymer electrolytes, especially PEO-based electrolytes, combine high mechanical resistance with a high chemical stability against lithium.[66] However, their ionic conductivity is limited at room temperature and therefore need to be heated to allow for acceptable cycle rates which decreases their mechanical stability.[67] Dollé et al. [28] observed dendrites that penetrated the polymer electrolyte and short circuit their PEO / LiTFSI cell system.

Stack pressure

Applying mechanical pressure on the cell in is known to improve the cycling efficiency. It is assumed that the structural confinement prevents lithium dendrites from getting isolated from the electrode during lithium dissolution (i.e. during discharge in terms of a cell) by pushing them back into the lithium electrode, as lithium metal is soft (modulus $E_{lithium}$= 5 GPa) and very easily deformable.[68] The solid electrolyte and the mechanical force represents a growth restriction for growing dendrites and hence counteracts the growth away from the electrode.[69]

Operating temperature

Two different effects of the operating temperature on the cycling behavior of lithium electrodes have been reported and are apparently contradicting. Park et al. [70] reported that increasing the cell temperature from -5 °C to 35 °C also increased dendrite growth speed and hence decreased the cycle life of the cell. They used a 1 M $LiPF_6$ in the volume ratio of 1:1:1 for ethylene carbonate (EC), dimethyl carbonate (DMC), and ethyl methyl carbonate (EMC) electrolyte solution. In contrast to that, Mogi et al. [71] found that increasing the operating temperature to 80 °C increases cycling efficiency and forms smoother deposits. They argued that in the 1 M LiBETI/PC electrolyte they used and at elevated temperature, the SEI forms faster during the first cycle

and also repairs itself faster upon prolonged cycling. Li et al. [72] commented on both results and concluded that the elevated temperature can have two counteracting effects on the cycle life. While the increased temperature expedites SEI formation and repair, it also increases lithium ion diffusivity which might accelerate dendrite growth. Which effect becomes dominant would then be determined by factors like the type of electrolyte.

2.2.8 Non-Electrochemical 1D Growth Mechanisms

Several growth mechanisms in metals for one-dimensional structures have been reported. These are not directly related to lithium or to electrodeposition but the underlying mechanisms are mentioned here since they may have some applicability for the electrodeposition of lithium. On the one hand, some of these mechanisms cause filaments to grow accidentally and pose an unwanted reliability and safety issue. On the other hand, some of the mechanisms are applied on purpose to manufacture filaments.

Whiskers

The most prominent accidental 1D metal growth is the tin whisker growth at solder points. These whiskers can reach lengths in the millimeter range. They tend form spontaneously after extended periods of time. The underlying mechanism was described as combination of the formation of an intermetallic phase, stress relaxation and long range atom diffusion along grain boundaries.[73] At a solder joint, tin as the soldering material forms a layer over the copper wiring of the electric circuit. At the copper/tin interface, an intermetallic layer begins to form, causing mechanical stress in the tin layer due to the asymmetric interdiffusivity of Cu and Sn. The tin layer releases stress by long range atom transport out of the compressive areas via grain boundary diffusion. Grain boundaries with a horizontal component allow for the incorporation of atoms at lower stress than vertical grain bounda-

ries (of e.g. columnar grains). The grains at the tin surface that are associated with the boundaries with horizontal component then become pushed upwards, as more and more atoms are deposited at their grain boundary. Consequently, the resulting whisker is growing from its base and has the diameter of the grain where it originated. For other materials, the mechanism of stress relief by material transport over grain boundaries towards the surface might also be applicable.[74]. Whiskers were also observed for cadmium, zinc [74], silver [75], gold [76], aluminum [77], lead [78] and indium [78].

Vapor-liquid-solid method (VLS)

Driven by the miniaturization of electronics, sensors and optics, research has been devoted towards the controlled fabrication of 1D metal and semi-conductor structures. A very common technique in this field is the vapor liquid solid method (VLS). The VLS method for nanowire growth will be explained by using the example of a common fabrication route for silicon nanowires.[79] Small droplets in the nanometer range of a metal that is known to alloy with silicon (usually gold) have to be finely dispersed on a silicon substrate. The substrate is then heated above the eutectic temperature of the Si-Au alloy which allows the formation of eutectic Au-Si liquid alloy droplets. Impingement by silane then leads to a supersaturation of the liquid alloy with silicon that causes the excess silicon to precipitate underneath the droplet. This way, a silicon nanowire with the diameter of the droplet is growing underneath the liquid alloy droplet. This process is also applicable for growing nanowires of e.g. Ge, SiC and ZnO.[80] Lee et al. [81] discovered the method of oxide-assisted growth that uses silicon oxides instead of gold as a nucleation point. With this method silicon nanowires can be grown without metal impurities.

Nanowhisker growth by PVD

A way of growing one-dimensional metal nanostructures without mechanical stresses or alloying was introduced by Richter et al. [6, 82] They used various heated substrates (e.g. oxidized silicon wafers and tungsten foils at about 0.65 T_m of the whisker material) and covered them by a 30 nm thin carbon layer. Physical vapor deposition (PVD) of a metal onto the substrates resulted in the growth of a wide range of metals nanowhiskers. Based on the model theory of Ruth and Hirth [83] they identified the carbon coating as the key factor in their observed growth mechanism: Two different surfaces are needed to initiate the nanowhisker growth. One is the carbon coating that spreads over the majority of the substrate and represents an area with a low surface energy and high interface energy with the deposited whisker material [82] The carbon coating does not create a continuous layer, so the small fraction of the substrate that was not covered by carbon serves as an area of high surface energy combined with low interface energy with the deposited material. These holes in the carbon coating that reveal the substrate then act as nucleation point for the deposited whisker material.[6] Once the lateral growth of the nuclei reaches the boundary of the carbon layer, the high interface energy between the substrate and the deposited material then starts to hinder further lateral growth. It is important that the metal of choice does not wet the carbon layer; in the case of cobalt which wets carbon no whiskers were observed. However, they were able to grow cobalt nanowires on a CaF substrate, as CaF is not wetted by cobalt.[82]

2.2.9 Summary and Motivation

Many explanations for the formation and growth of whiskers exist. Some of the attempts even contradict each other and some are not compatible with the published experimental results: The

models based on the ionic transport in solution (spherical vs. planar diffusion, concentration gradient, edge effect) assume that a dendrite grows at its tip. The observations of Yamaki et al. [62] and Crowther and West [25] clearly demonstrate that the growth does not occur exclusively at the tip, however, their observations were limited to dendritic bushes. Yamaki et al. proposed the only theory describing the growth from the base, but has been criticized by Monroe and Newman [54] for their questionable assumptions on the flow behavior of lithium. In addition, they did not observe elongation by deposition at the tip, and consequently their model does only incorporate growth at the base. However, Crowther and West [25] suggested that both growth locations are active for dendrite bushes. The exact locations of the growth points have not been determined so far, in particular, for the simplest case of needles.

It was clearly shown by the experimental results that the current density has a major influence on dendrite formation and growth, but the exact predictions for different current densities are contradicting. While Dollé et al. [28] found that the morphology changes from moss-like to needle-like with increasing current density, Brissot et al. [21] observed the opposite namely less needles and more bushes/moss at higher current densities. The growth speed of dendrites was also clearly shown to be linked to the current density, but the growth speed predictions are also contradicting. For example, Barton and Bockris [16] predict a constant dendrite growth speed that is proportional to the current density. Monroe and Newman [54] also predict higher growth speeds with increasing current density, but they expect the dendrite growth to accelerate over time. Chazalviel et al. [20] calculated a dendrite growth speed that is proportional to the electric field, but does not change with time.

Electrolyte composition and additives have also shown to have a major influence on dendrite growth. However, although a high number of electrolyte compositions have been investigated, the success in suppressing dendrites is rather limited. Aurbach et al. stated that there is no way a lithium electrode can be passivated well enough by careful electrolyte design so that it would be able to compete with graphite-based anodes during cycling at high rates.[84]

2.3 Objectives of This Work

Lithium dendrite growth is known since the 1960s, but despite all effort that was put into mitigating this problem, it still prevents the commercialization of lithium metal anodes and also haunts today's lithium-ion systems. The attempts of suppressing the formation and growth have only shown little success as the understanding of the fundamentals of this problem is still very limited. As it was recently put, "future work (…) needs to focus more on addressing the origin of the problems instead of only on consequences of the problems" [5], since the literature on this topic is contradicting even on rather basic questions.

The experimental evidence of this phenomenon is often based on light microscopy observations. Due to the high refractive index of the electrolyte and the rather poor optical conditions in the test cells, the spatial resolution of the data in the literature is not adequate for identifying microscopic effects. The aim of this work is to develop optimized *in situ* cells for light microscopy and observe the lithium plating process at the highest spatial resolution. The aim is to study the mechanisms behind dendrite growth and to find possible strategies to suppress dendrite growth. Chapter 4 addresses the surfaces on lithium deposits and gives indications on the growth direction of needles. In chapter 5, the controversial question at which sites lithium dendrites grow is

treated by studying the example of lithium needles. Video recordings of unmatched resolution were obtained in dedicated cells optimized for light microscopy. A detailed insertion mechanism is described in this chapter to explain the observed growth. Chapter 6 deals with larger scale lithium deposits in the form of bush- or moss-like dendrites and investigates their growth and dissolution. Chapter 7 focuses on the influence of the substrate on the deposition behavior and further elucidates the role of the crystal lattice of the substrate on the formation and growth of needles. In chapter 8, the role of electrochemistry is investigated by comparing deposits created by thermal evaporation with electrochemically deposited structures.

The entire chapters 5 (see [1]) and 6 (see [2]) are already published as articles in peer reviewed Journals. Chapter 8, apart from the footnote concerning substrate grain orientation, has been submitted (see [3]).

3 Experimental

3.1 Substrates

Lithium deposition was carried out in different setups on various substrates. The substrates needed to be electrically conductive and electrochemically stable down to -3.04 V vs. a standard hydrogen electrode (the electrochemical potential of lithium). In addition, surface oxides as well as surface roughness had to be avoided to exclude their influence on the deposition. Consequently, three different substrate types were mostly used (Fig. 3.1). The first substrate type was tungsten films (image a). These films were created by sputter-depositing tungsten to a thickness of 10 nm onto borosilicate microscope slides. Various shapes of the substrate could be realized by the lift-off technique (with scotch tape) as well as by cutting the microscope slide to shape with a diamond glass cutter. Using a Leica transfer shuttle, the substrate could be transferred from the sputter coater to the glove box without contact to atmosphere. The other substrates were copper substrates. They were either cut into rectangular shape (image b, similar to the tungsten film samples) or lathed from a copper rod (Alfa Aesar, Puratronic 99.999 %) into a round, hat-like shape (image c). The hat shape allowed the transfer into an STM (University Ulm) as well as the fixation of these samples in a home-built polishing holder (Fig. 3.2). This polishing holder secured the samples mechanically which allowed grinding and polishing the samples without the need for gluing or embedding into a resin (as it was needed for the rectangular copper samples). This helped avoiding contamination of the samples and the cell with residual polymers. The holder was also designed to be used in the vibratory polisher. In order to reduce surface oxides, the copper samples were exposed to a forming gas atmosphere (5 % H2 und 95 % Ar)

at about 250 °C for 15 minutes. This was performed in the large load lock of a glove box, so that contact with the atmosphere after the reduction of the oxides could be avoided.

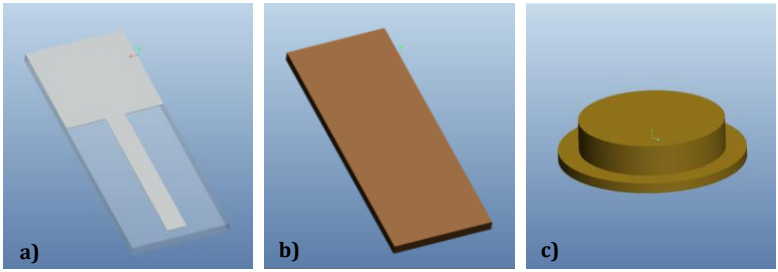

Fig. 3.1: Substrates used for electrochemical deposition of lithium. Image a) shows a structured tungsten film on a borosilicate substrate, b) shows a rectangular copper substrate and c) a hat-shaped copper substrate.

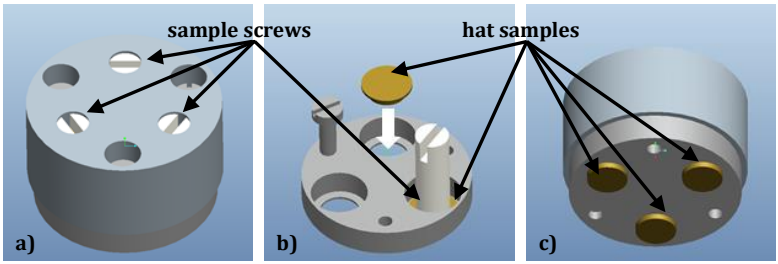

Fig. 3.2: Two-part polishing holder for three hat-shaped samples (**a**). The lower part (**b**) has three apertures to accommodate the samples; the sample screws are screwed into the upper part and push the samples into their apertures. The other screws secure the lower part against the upper part. The samples protrude about 1 mm from the holder in the unpolished state (**c**).

3.2 Electrolytes

Mainly two different electrolytes were used. The first one was a 1 M solution of $LiPF_6$ in a 1:1 weight ration mixture of EC and DMC. This is a standard electrolyte for lithium-ion batteries and is a commercial electrolyte sold by BASF under the product name LP30. According to the manufacturer, the hydrofluoric acid content is below 50 ppm and the water content below 20 ppm. The second electrolyte was a 1 M solution of Li[CF3SO2)2N] (LiTFSI) in 1,3-dioxolane (DOL): dimethoxyethane (DME) (1:1 by volume) provided by BELLA (Battery and Electrochemistry Laboratory) with less than 20 ppm of water as determined by Karl Fischer titration. While $LiPF_6$ electrolytes form a more salt-based SEI, LiTFSI salt based electrolytes are expected to form a more solvent-based SEI.[85] In addition, DOL was reported to form a more flexible SEI on the anode due to the high elastomer content.[43] Consequently, LiTFSI-in-DOL electrolytes are well suited for anodes that undergo strong volume changes (silicon) or strongly localized volume changes (lithium metal, especially in Li-S systems), since a flexible SEI is required to ensure reliable passivation of the electrode during prolonged cycling. For Li-S systems, DME is added as it offers a higher polysulfide solubility and faster polysulfide reaction kinetics than DOL, while DOL is still needed as it forms a more stable SEI.[86] In addition, most other common electrolyte solvents were reported to react with the polysulfides.[87] These two very distinctly different electrolytes were chosen in order to investigate the effect of the electrolyte and the SEI on the deposition.

3.3 *Ex Situ* Cell

Conventional Swagelok cells could not be used for *ex situ* deposition experiments, as they require mechanical pressure on the electrodes and a separator which would both interfere with the

growth of dendrites. Therefore, a home-build cell setup was designed to be operated inside the glove box (Fig. 3.3). In this setup the substrate was immersed into the electrolyte inside a beaker without any restriction for the dendrite growth. However, this design led to the following problem: The electrolyte solvents are volatile, so an open cell setup could not only lead to a contamination by possible impurities in the glove box atmosphere, but more importantly to a decreasing electrolyte level and as a result to an increasing salt concentration. Therefore, the system was designed to be gas tight while maintaining easy working electrode replacement. In addition, the amount of gas volume inside the cell was minimized to cause the gas pressure inside the cell to rise faster during solvent evaporation keeping the evaporation to a minimum.

The working electrodes in our setup were the copper and tungsten substrates (see 3.1). They could be dipped vertically into the electrolyte or they could be inserted with their surface in parallel to the electrolyte surface creating a hanging meniscus. In the case of the vertical insertion, a higher current concentration and increased deposition on areas of the substrate close to the electrolyte surface were observed. Although the exact reason for this could not be determined, it was probably related to effects similar to the "coffee ring" effect.[88, 89] Using the hanging meniscus technique, this effect could be circumvented and homogenous covering of the surface was obtained.

Lithium metal foil (1 mm thick, 99.9 % from Alfa Aesar) was used as counter and reference electrodes. Measuring the potential between the reference and the working electrode instead of measuring the potential between the counter and the working electrode allows the accurate measurement of potentials by excluding the potentials drops from the Ohmic resistance deriving from the electrolyte or from the counter electrode surface layer. A

third lithium metal electrode was used in order to validate the potential of the other lithium metal electrodes. This way, a faulty or contaminated lithium electrode could be easily identified and replaced.

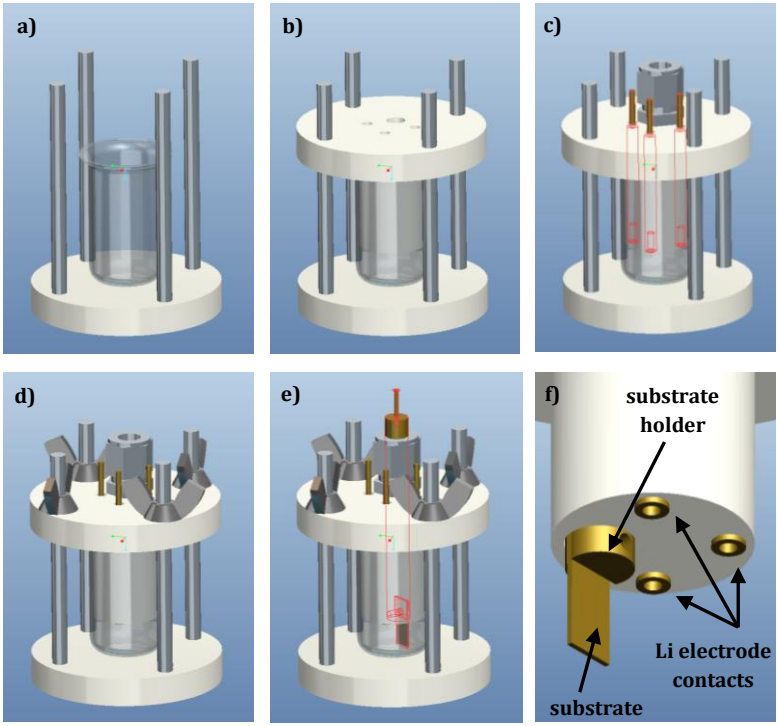

Fig. 3.3: *Ex situ* cell setup. A borosilicate beaker (a) is used as a container for the electrolyte; the lid (b) seals the beaker (with an O-ring) and has four holes for electrode feedthroughs. The thinner part of the lid reaches into the beaker and fills up most of its volume to reduce the amount of gas inside. Three copper rods (c) are screwed into the lid as fixed feed-throughs for the lithium electrodes. A pipe connector (c) serves as a fixation and seal for the sample holder (e and also Fig. 3.4). The substrate holder has a slit where tungsten-film substrates can be fitted (f). With this holder, the substrates are dipped vertically into the electrolyte. Li metal electrodes are screwed into the Li electrode contacts (f).

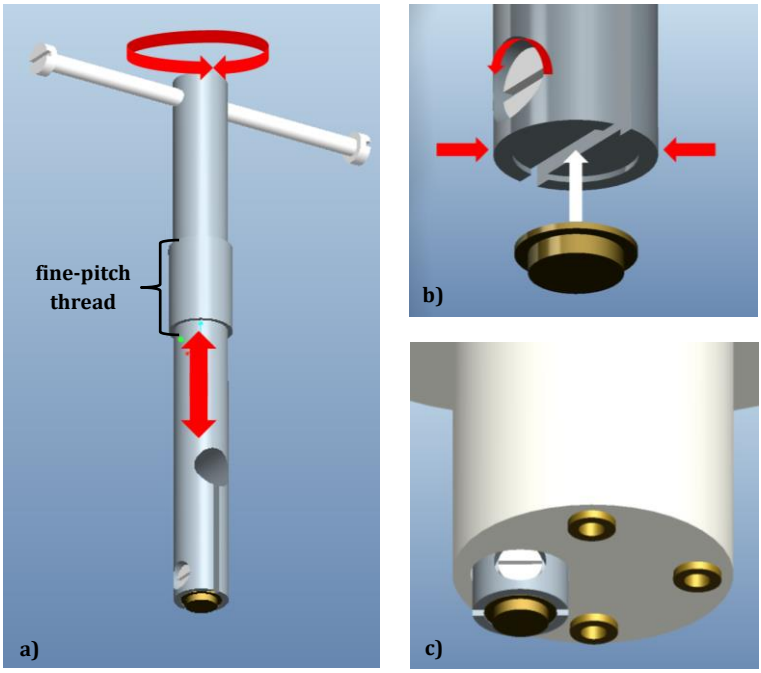

Fig. 3.4: Sample holder for hat shaped samples (**a**). Instead of using friction between the holder and the pipe connector (as for the sample holder in Fig. 3.3), both the holder and the pipe connector were equipped with fine-pitch threads. With this, the immersion depth of the substrate could be precisely controlled by rotating the holder. The samples were clamped to the holder by tightening a screw located at the side of the holder (**b**). With this holder, the samples are immersed parallel to the electrolyte surface (**c**).

3.4 *In Situ* Cell

As the electrolyte is opaque to electrons, we had to rely on light microscopy to perform *in situ* studies of lithium dendrite growth inside a liquid electrolyte (Fig. 3.5). The *in situ* cell consists of two tungsten current collectors sputtered onto a glass slide, a 0.2 mm

thick polyethylene (PE) frame as spacer and a 0.17 mm thick cover glass. A piece of lithium was placed onto the tip of one current collector (a), and the PE frame was melted to the glass slide surrounding both current collector tips (b) with a cover glass on top (c). This way, the frame between the cover glass and the glass slide created an empty space with two openings. The cell was filled with electrolyte by dripping electrolyte from a syringe onto one opening. The capillary force created by the thin cell interior (0.2 mm) strongly helped in this filling process.

The second opening allowed the gas trapped in the hollow space to escape. The electrolyte inside both openings was removed, so that only the center of the cell contained electrolyte. When the openings were then sealed, a gas bubble would avoid direct contact of the battery sealant with the electrolyte. By avoiding electrolyte contact with the battery sealant (that is also why the PE was melted onto the glass instead of glued with sealant) the lifetime of the cells could be extended from several days to more than a week. Once the sealant was dried, two-component epoxy was additionally applied on top of the melt and glue joints to mechanically strengthen the cell and support adhesion. The flat sputtered electrodes not only provided smooth oxide and water free metal surfaces, they also helped in improving the imaging quality as the entire surface could be in focus even at high magnification. The very thin cell design also limited the detrimental effect of the liquid on the optical resolution. The deposition area was the part of the tungsten film that was not covered by the PE frame (c). The area of this exposed surface was minimized by minimizing the width of the tungsten film and the channel in the PE. This way, the majority of the deposition area could by monitored in one frame.

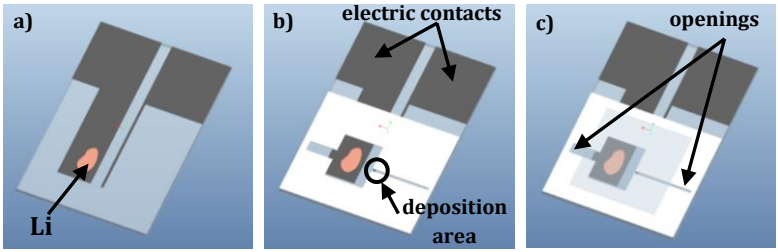

Fig. 3.5: *In situ* optical cell. Structured tungsten films are deposited by sputter coating (dark grey). These films act as current collectors and substrates; lithium (red) is then put on the tip of the wider film. This film is the counter electrode. A polyethylene frame (**b**) and a cover glass (**c**) are attached by heating the cell slightly above the melting point of PE and applying mechanical pressure. Electrolyte is then dripped onto the larger channel in the PE frame; capillary force drags the fluid into the cell while the gas inside cell can escape through the thin channel. Both channels are sealed with battery sealant; the entire cell is mechanical reinforced with two-component epoxy afterwards. The thin film that remains exposed inside the channel becomes the deposition area (**c**).

4 Crystallinity and Growth Direction

Lithium was electrodeposited in the *ex situ* beaker cell on tungsten films and on vibratory polished copper. The deposition was carried out potentiostatically at -100 mV vs. Li for 100 s.

4.1 Results

The resulting deposits were imaged by SEM and are shown in image a) of **Fig. 4.1**. Needles and faceted particles were observed and often needles grew directly from the particles as shown in **Fig. 4.1** b). **Fig. 4.2** a) and c) shows the two most commonly observed shapes of the facetted particles. However, sometimes the shape of the particles deviated from these presented shapes by slight distortion. **Fig. 4.3** shows that the needles growing on the side facets of particles were most likely growing parallel to the substrate. Image b) shows the tip of such a needle; by cutting away the tip an area of the substrate film is revealed that seems to have bulged and cracked as the dendrite hit it during its growth (image c)).

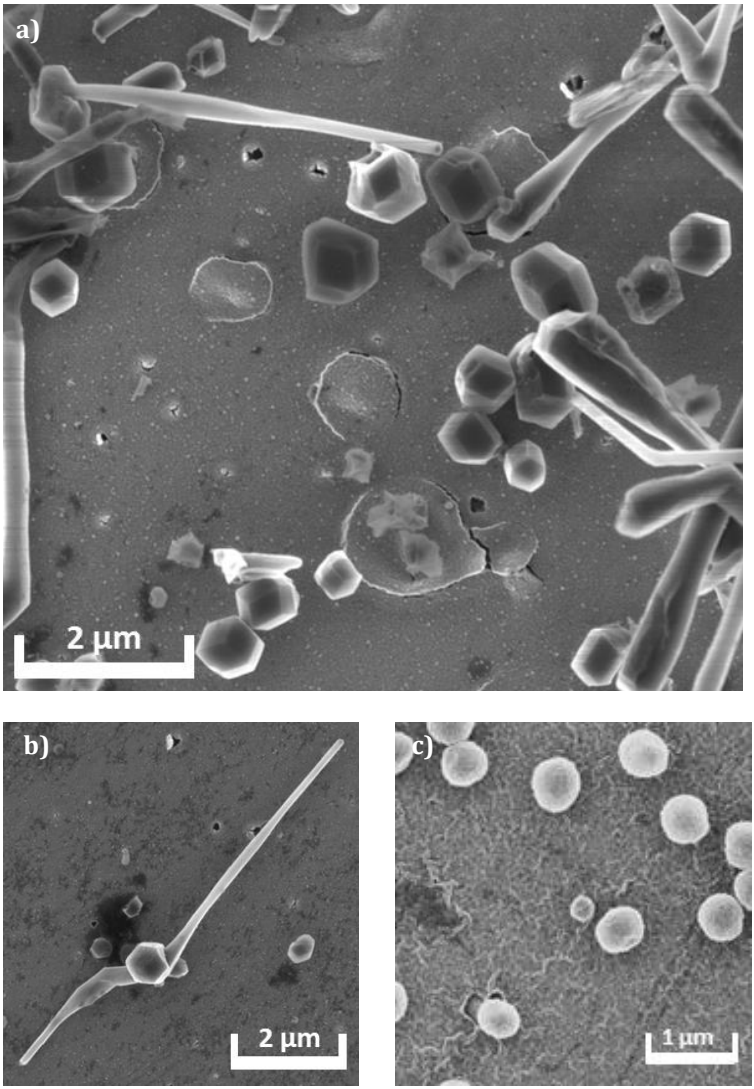

Fig. 4.1: SEM image of needles and facetted particles after deposition at -100 mV vs. Li for 100 s (a). Needles were observed to grow from these facetted particles (b). Round particles were observed after galvanostatic deposition(c).

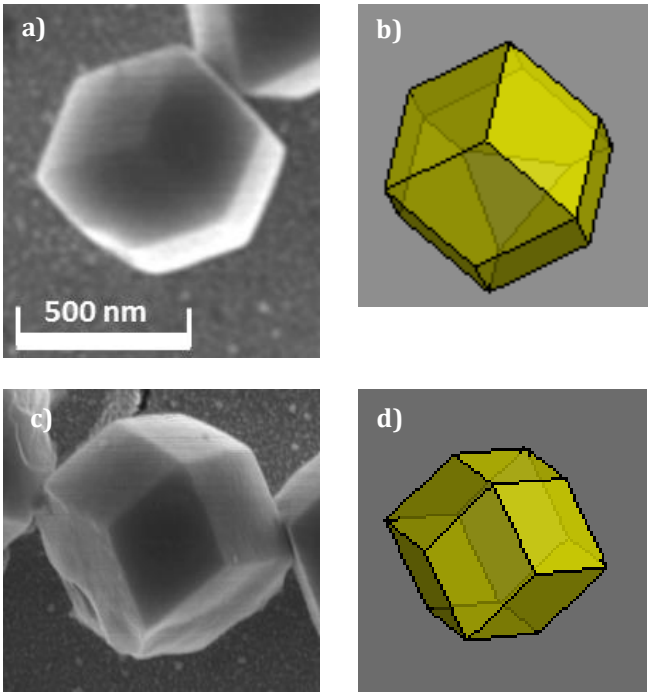

Fig. 4.2: Images a and c show the two shapes of facetted particles that were observed. Images b and d show Wulff shapes with {110} planes exclusively that were oriented to mimic the corresponding lithium particle. The shape in image d) is the same shape of image b) but was slightly rotated. The substrate is drawn in grey. The Wulff shapes were calculated using the software *Wulffmaker* [90].

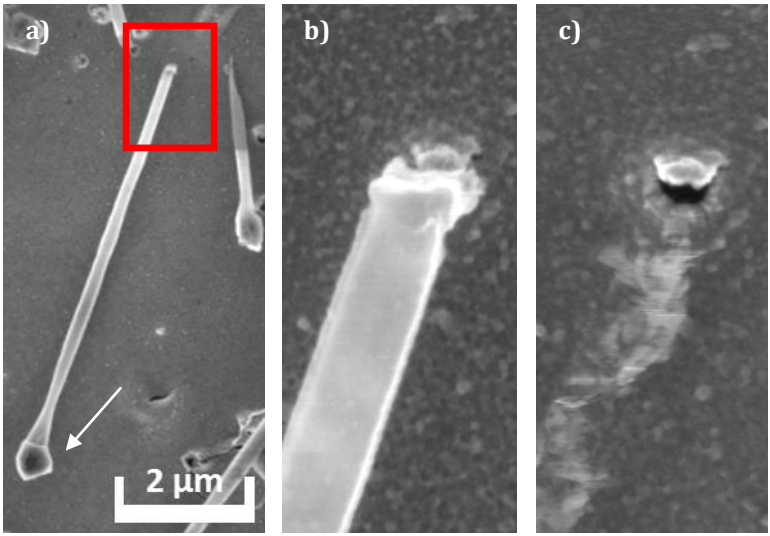

Fig. 4.3: SEM image of a distorted facetted particle (arrow in a). A needle is growing from the particle; the tip is shown in image b. After having cut away the tip with the electron beam, a location on the substrate where the tip hit the substrate during growth becomes visible. This means the needle had grown almost parallel to the substrate.

4.2 Discussion

Finding facetted electrodeposited lithium particles strongly suggests that these particles are crystalline. Conventional methods for determining crystallinity are extremely difficult to apply to lithium due to its extremely low density (i.e. weak electron and x-ray interaction) and high reactivity. To determine which crystal plane correlates with the facets, Wulff shapes were calculated using the software *Wulffmaker* [90] and compared to the observed facets on the particles. **Fig. 4.4** shows Wulff shapes constructed with different crystal planes.

In order to verify if the observed facets could correspond to certain crystallographic planes, several Wulff shapes with low index facets were calculated (**Fig. 4.4**). The comparison of the observed lithium particle shape in **Fig. 4.2** a) to the Wulff shapes in **Fig. 4.4** shows the strong similarity between the lithium particle and the {110} facetted Wulff shape (**Fig. 4.4** b). A corresponding Wulff shape with {110} facets is shown in **Fig. 4.2** b) for better comparison. By slight rotation of this Wulff shape, the shape of image d) in **Fig. 4.2** is obtained. This shape resembles the other lithium particle shape shown in image c). This means that we probably observed {110} facetted lithium particles exclusively. The crystallization of electrodeposited lithium in Wulff shapes suggests that the observed lithium particles are single crystals. In addition, this suggests the {110} planes of lithium seem to have the lowest interface energy and hence that they are thermodynamically preferred, i.e. that the lithium particle forms according to the Wulff construction in order to reduce its free energy. Often, the shapes of deposits depend on the growth kinetics, i.e. they depend rather on the progression rates of different facets than on their stability. Suggesting thermodynamic control here is based on the assumption of fast rearrangement of the lithium atoms which may be justified based on the results presented in chapter 8.

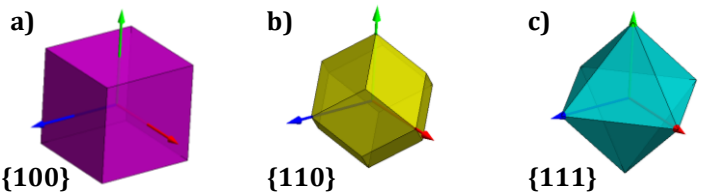

Fig. 4.4: Wulff shapes composed of {100} planes in image a), {110} planes in b) and {111} planes in c). The arrows mark the <100> axes. The shapes were calculated by using the software *Wulffmaker* [90] and assuming that the surface energy of the dominant planes is two times smaller than the surface energy of the other planes.

The surface energy per area of the {100} planes were calculated to be lower than for {110} planes [91] which contradicts our observation. However, these calculations neglect the existence of the SEI and the electrolyte, which is why we assume they are responsible for the formation of {110} instead of {100} planes. For example, the interface energies between lithium and the SEI as well as possible adsorbates contained in the electrolyte might play a dominant role. Adsorbates modify the surface energies of metals which can result in a dependence of the Wulff shapes on the adsorbate chemical potential, see e.g. [92]. To further elucidate the role of the SEI, we compared the particles obtained by potentiostatic deposition with particles obtained for galvanostatic deposition at comparable rates (**Fig. 4.1** c). During galvanostatic deposition, the SEI is expected to form before the reduction potential of Li^+ is reached. This means deposition takes place after a SEI has formed on the substrate and that lithium is plated underneath an existing SEI. That way no direct interface between the lithium and the electrolyte is expected during the process. In addition, the SEI needs to be deformed as the lithium particles from underneath it; this might restrict the growth of the particles and the formation of facets mechanically. As a result, particles formed during galvanostatic conditions were observed to be non-faceted and hemispherical. During potentiostatic deposition at constant potential, the voltage jumps directly to the deposition potential, so the SEI formation and the Li deposition should take place simultaneously. This means that instead of depositing lithium underneath an existing SEI, the SEI forms on the lithium particle while it is growing. This way, the particle is less restricted in its growth and might also have an electrolyte-lithium interface for a short time before an SEI forms. Hence, we suggest that the formation {110} facets might be triggered by two factors: little or no mechanical restriction through the SEI (enabling faceting at all) and adsorbates on the lithium surface (modifying the surface energy so that {110} facets form instead of {100}).

The SEI may be the reason why not all observed particles show the idealized shapes of **Fig. 4.2** b) and d), as it interferes with the particles tendency to form {110} facetted Wulff shape when in contact with the electrolyte. Hence we suggest that the pronounced {110} facets only form when the growth of the particles is not restricted. Furthermore, fast lithium diffusion is required to obtain equilibrium shapes, which might be the case when there is a direct electrolyte-lithium interface. These results suggest that the {110} plane of lithium has the smallest lithium/electrolyte interface energy. Langenhuizen [93] also reported facetted particles in a 1 M $LiPF_6$ in EC:DEC electrolyte. However, the presented resolution of the SEM images was too low to identify the facets correctly. The facets were observed to disappear when the HF content was increased from 6 to 60 ppm – another indication of the influence of the SEI and the electrolyte.

Depicted in **Fig. 4.5** is the needle growing on a facetted particle as shown in **Fig. 4.3** b). There are two needles growing on it. One shows faceting at the root close to the substrate (see **Fig. 4.5** b), while the faceting seems to fade with increasing distance from the root. The needle seems to share a facet with the particle (see arrows in b)), a phenomenon commonly observed under these deposition conditions. Assuming homoepitaxial growth of the needle on the particle, this would mean that the needle preferably forms the same facets, but the influence of the SEI seems to become stronger with time while the needle elongates. This could probably cause the fading of the facets along the length of the needle.

Knowing that needles from particles probably grow parallel to the substrate (which is suggested by **Fig. 4.3**) in combination with the identification of the facets and the orientation of the single-crystalline lithium particles makes it possible to identify the growth direction of the needles growing from these particles. This

is shown in **Fig. 4.5**. Image c) shows the calculated Wulff shape of the particle in b). The orientation of the particle was used to calculate the corresponding low index directions, shown in d), e) and f). The marked [111] direction of image f) appears to be the only low index direction that points in the growth direction of the needle. Hence, we suggest that the observed needles grow along the <111> direction.

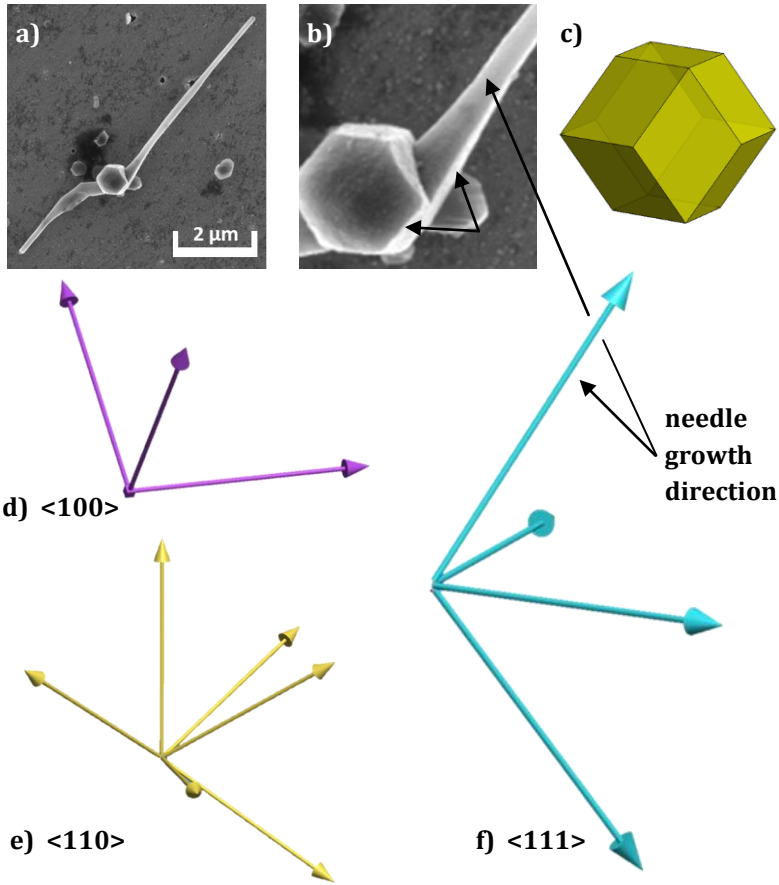

Fig. 4.5: (a) SEM image of a facetted lithium particle with two needles growing from it. (b) SEM image of the same particle shows that the needle is also facetted at its root. The side facet of the needle seems to be a continuation of the side facet of the particle. Also the top facet of the needle seems to be same as one of the top facets of the particle. (c) Wulff shape mimicking the faceting and the orientation of the particle. The colored arrows in (d), (e) and (f) mark the low index directions in the same orientation as image c). Image (f) shows that the marked [111] direction is the only low index direction that comes into consideration as the growth direction of the needle.

5 Mechanism of Needle Growth

Lithium needle deposition inside *in situ* cells was monitored by light microscopy and by *ex situ* SEM. Current and potential were supplied and monitored by a portable potentiostat/galvanostat. The growth of dendrites could be observed *in situ* with unmatched resolution. This chapter was published in [1].

5.1 Results

Fig. 5.1 shows a typical galvanostatic voltage vs. time plot of lithium deposition on a tungsten substrate. The initial open circuit voltage was around 1.5 V and started to drop once a negative current was applied. The curve started to change slope between 1 V and 0.5 V and after a slight negative peak, the first plated structures became visible on the substrate. The voltage asymptotically approached a small negative value while deposition. Upon change of the direction of the current, the dissolution was visually observed. During lithium dissolution the voltage remained at a similar absolute value than during deposition but stayed positive. After a while the voltage rose. When reaching 2.5 V, the electrical circuit was opened and during relaxation a potential of 2 V was asymptotically approached.

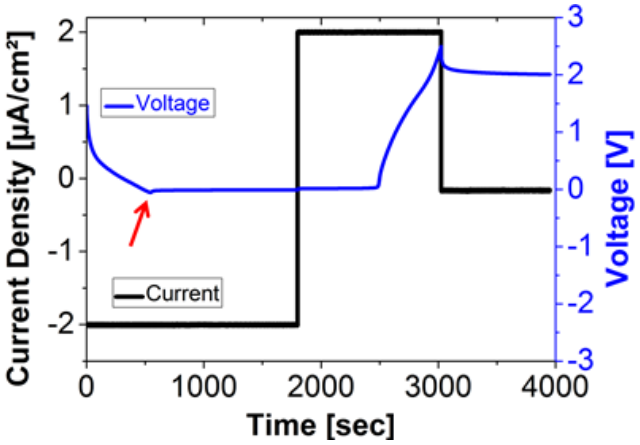

Fig. 5.1: Galvanostatic voltage vs. time plot of a glass cell with a sputtered tungsten substrate. The red arrow marks a potential peak. The current density is related to the exposed tungsten working electrode area.

We observed the growth of needle-like lithium on tungsten substrates via *in situ* light microscopy. The needles either grew directly on the tungsten substrate (**Fig. 5.2**) or from larger lithium particles (Fig. 4). During growth, an increase in diameter was not observed, while they significantly gained in length. The needles consisted of several straight linear segments of a few microns in length and kinks between these segments. No preferred growth direction was found, e.g. the needle in Fig. 4 grew almost parallel to the substrate while the needle from Fig. 3 grew away from the substrate.

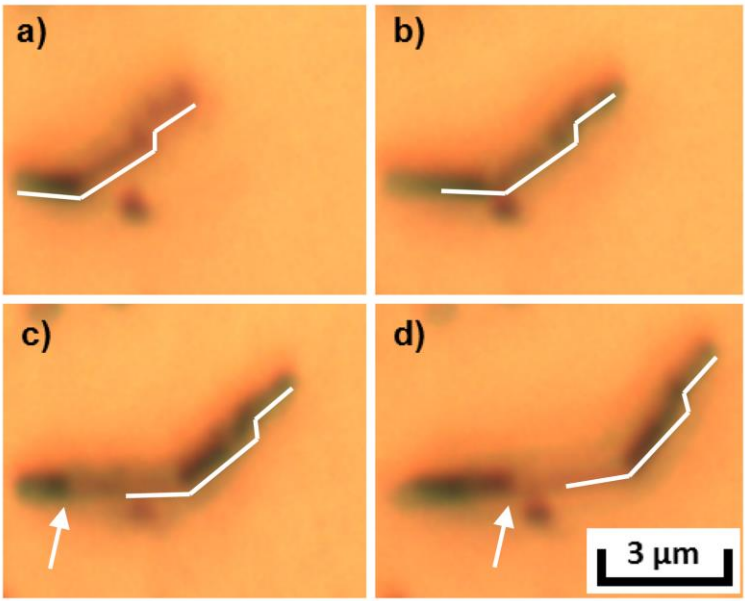

Fig. 5.2: *In situ* light microscopy of needle-like lithium growth in 1 M $LiPF_6$ electrolyte. The structure of image a) (traced in white) remains unchanged, while more segments are added at the base of the structure as shown in the subsequent pictures, i.e. the images demonstrate that in this case the growth occurred exclusively at the base of the needle. A kink forms in c) and is marked by an arrow. Image b) was taken after 15 seconds, c) after 180 s, and d) after 450 s after figure a) was recorded.

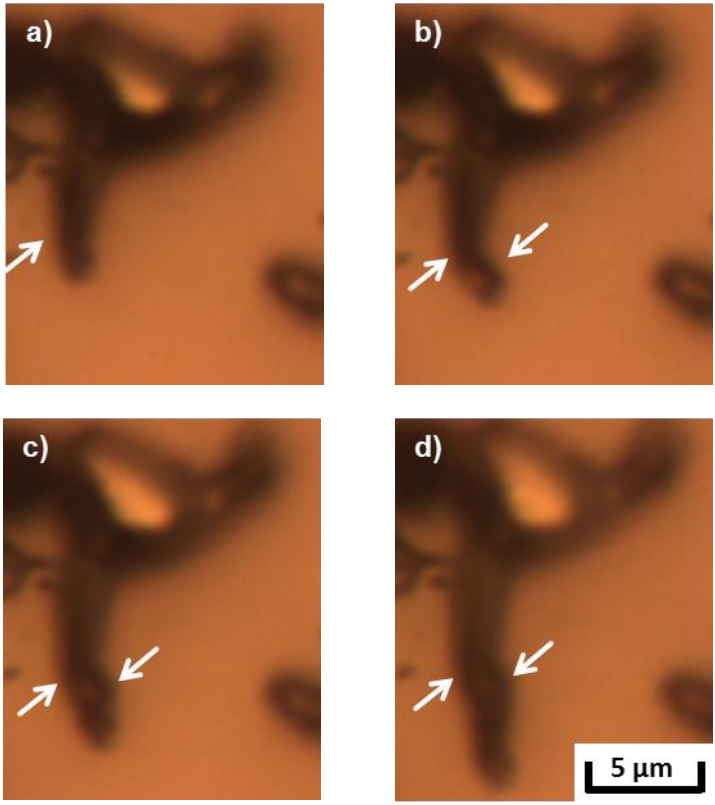

Fig. 5.3: *In situ* light microscopy of needle-like lithium growth in 1 M $LiPF_6$. Image a) shows needle-like lithium. The needle forms a kink (marked) in image a) and another kink (marked) in image b). Image c) and d) show that during further growth the size and position of the needle segments and kinks did not change, instead the tip segment of the needle grew in length. Image b) was taken after 105 s, c) after 195 s, and d) after 360 s.

Fig. 5.2 shows the growth of a needle that grew at the base. The long tip structure of **Fig. 5.2** a) (traced in white) remained unchanged throughout the entire growth of the needle, while the part of the needle that was close to the substrate increased in length. In b) it can be seen that the segment at the base gained in length. In picture c) of **Fig. 5.2**, the arrow marks a kink that formed at the base of the needle. In d) the kink had moved forward in the direction of growth. Needles were also observed to grow by adding material to the tip. In **Fig. 5.3** a) another needle that grew from a larger particle is shown (see also Video S 1[2]). It exhibits a kink, marked by an arrow. During its growth, it formed an additional kink as shown in b). Contrary to **Fig. 5.2**, the kinks stayed and did not move during further growth as can be seen for example by comparing c) and d). This observation is indicative of tip growth because growth at the base would have caused motion of the kinks as was observed in **Fig. 5.2**. Besides growth at the base and growth at the tip also growth can happen between kinks. **Fig. 5.4** shows a filament structure with two pronounced kinks. During lithium deposition, the segment between the kinks elongates. In some cases, the extension between kinks was associated by a change in the kink angles which can be seen by comparing a) with c). We also found lithium filaments that simultaneously grew at several points including base, top and in between kinks. For example, a needle has been observed with three segments that gained in length at the same time. Although these three different growth sites can be clearly identified, from the observations it seems that growth at the base was most common. Growth at the top and in between two kinks was somewhat less common.

[2] The video can be found online in the supplementary info of [78].

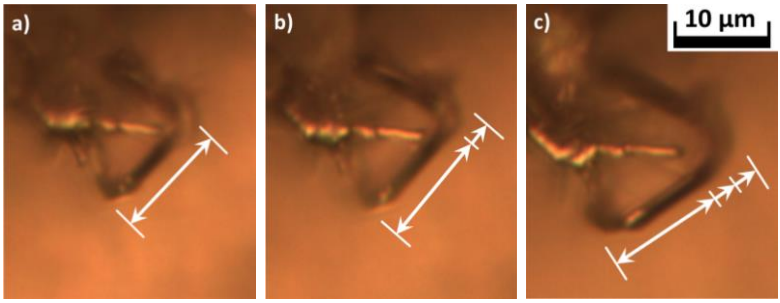

Fig. 5.4: *In situ* light microscopy of needle-like growth in 1 M $LiPF_6$ on a lithium substrate. The view on the tip and the base of the needle is obstructed by other lithium structures; three straight segments connected by two kinks can be seen. Images b) and c) show that the segment between the kinks grew in length (marked by white arrow). Image b) was taken after 45 s, and c) after 135 s.

According to the voltage vs. time plot (**Fig. 5.1**) a significant amount of the plated lithium could be dissolved (~55 %). In the case of the dissolution of a lithium filament, the tip was left behind only connected to the substrate by a thin wire-like structure (**Fig. 5.5** and Video S 2[3]). Both, this tip and the thin connecting remnants could not be dissolved. The dissolution started in the vicinity of the tip, thinning the needle locally. As dissolution progressed, the thinned area moved downwards, similar to the sharpening of a pencil, while the tip itself did not change its position.

[3] The video can be found online in the supplementary info of [78].

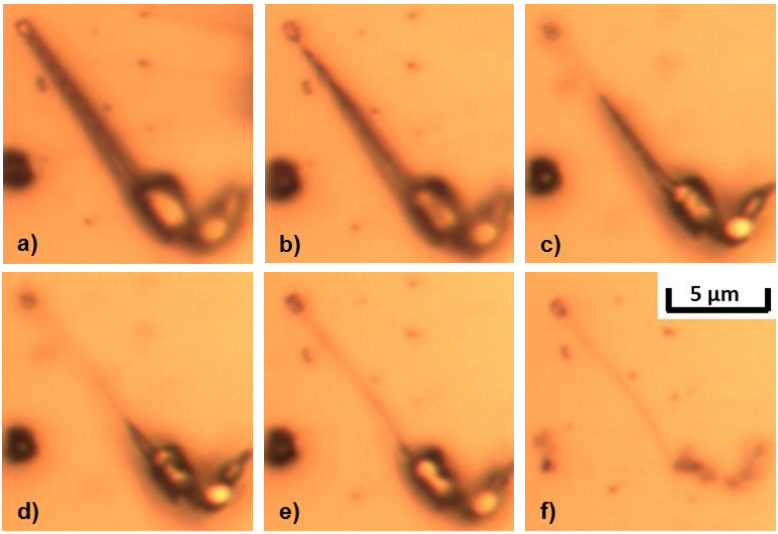

Fig. 5.5: *In situ* light microscopy of the electro-dissolution of a lithium needle. Image a) shows the initial needle and images b) to f) its dissolution. In image b) the dissolution is a thinning process localized to the area near the tip leaving a tapered needle. As this region is dissolved, the thinning area moves downwards, similar to the sharpening of a pencil. The tip and a thin wire could not be dissolved. Image b) was taken after 240 s, c) after 285 s, d) after 360 s, e) after 390 s, and f) after 585 s.

5.2 Discussion

Nishida et al. [94] claimed that the slight voltage peak (see red arrow in **Fig. 5.1**) is caused by a reduction of a thin surface oxide layer. Sagane et al. [95] attributed this peak to the nucleation and growth process since he observed that first precipitation occurred after the peak. This is also our interpretation, as we have observed this peak reoccurring during deposition following a complete dissolution of the Li. This peak was also absent during plating on Li metal where no nucleation process is expected. The change in

slope of the voltage curve below 1 V is interpreted as solvent decomposition and formation of the SEI.

The tip of a dissolving needle appears to be inactive, i.e. there is always distinct structure remaining after the lithium is dissolved. We suggest that the part that is inactive during dissolution might be also inactive during deposition, see Fig. A 1; hence, what appeared as deposition on the tip is rather a deposition of lithium between the inactive tip and the active lithium metal of the needle. The fact that lithium needles grew in length, but not in diameter, means that atoms are not attached to the sidewalls of the needle but instead are inserted close to the tip or at the needle-substrate interface. Growth between two kinks additionally suggests lithium insertion at kinks. Adding atoms always at the same location probably leads to the constant diameter of a segment. Our observations indicate that the growth of Li filaments is defect controlled and that lithium atoms are inserted into the crystal at defect sites. This suggests that conventional explanations based on field and concentration gradients are not adequate for the case of our experiments.

During deposition, the SEI forms on the freshly grown lithium while during dissolution, the SEI cannot be removed. This has important consequences when comparing deposition with dissolution. **Fig. 5.5** shows the removal of lithium along the needle and the persistence of the structure at the tip. This suggests that an SEI shell remains that holds the structure at the tip in the same position while the lithium inside this shell dissolves. The thin wire-like – supposedly tubular – structures of **Fig. 5.5** e) and f) that remained after dissolution are possibly these residues of SEI which are visible after the dissolution of the metal only because SEI attached to reflecting metal cannot be resolved by light microscopy. Although the dendrites were growing in length and not in diameter, the dissolution includes a thinning process starting at

the tip instead of a pure shortening process. Shortening of the whole structure might be impossible because of the constraints of the SEI shell.

The inactive tips may consist of metal oxides or lithium salt, e.g. LiF, or other impurities which can act as catalysts for lithium insertion. LiF crystals have roughly the size of a dendrite and resemble the shape of inactive needle tips.[96] This may explain why the tip shape of a needle does not change during growth, e.g. in Fig. A 1. Using synchrotron hard X-ray microtomography, small crystalline contaminants were found underneath every growing dendrites in a lithium polymer cell also indicating that contaminants may act as catalysts for dendrite growth.[97] In the literature, a flat and even distribution of LiF was observed to prevent dendritic deposition.[98] LiF was used here as an example. The inactive tip could for example also just be a relatively thick SEI layer locally grown on the lithium nucleus probably during onset of metal deposition, i.e. the parts (b) to (f) of the illustration remain valid for a growth without an initial extra structure as shown in (a).

5.3 Comparison to Other Models

None of the previously proposed models seem to be able to explain the growth behavior observed here. The model proposed by Cohen et al. [36] offers a conclusive explanation for dendrite growth initiation. The SEI also has been accepted as one of the major influences on dendrite growth.[36, 96, 98] However, crack formation in the SEI alone cannot explain why needle-like growth was observed instead of the growth of three dimensional bulk structures. On surfaces of freshly grown structures there is also a fresh, i.e. thin layer of SEI. If the resistivity or thickness of the SEI controls the growth, it can be expected that either growing filaments not only grow in length but also in diameter or that

branches nucleate on them more frequently. Furthermore, a deposition at the base of the structures seems unfavorable from the SEI point of view due to the thick SEI layer on the substrate. Defects of the SEI which may be present at kinks would result in a lithium deposition there, as illustrated by the round deposit shown in Fig. A 2 b). Lithium deposition at kink sites (shown as circular shapes in the model in [62]) was described explicitly for an LiAsF6 electrolyte by Yamaki et al. [62]; we did not observe such a deposition at kink sites for the 1 M LiPF6 solution.

The models featuring the ionic concentration gradient [19-21, 23, 55] predict a preferred growth direction into lithium ion rich areas of the electrolyte which is generally towards the counter electrode. In the case of our cell, the needles should have all grown towards the left in Fig. 3.5, but instead we observed what looks like a random distribution of growth directions. These models are also limited to deposition at the tip of a structure and hence fail to explain the observed atom insertion at the base. In addition, considering the current densities studied in our work, no significant concentration gradients are expected.

The growth predictions of the edge effect in electric fields [16, 54], the spherical diffusion flux [56, 57] and diffusion limited aggregation [99] are not limited to preferred growth directions, but are also limited to growth at the tip or at outer contours. In these cases deposition at the base of a needle is unfavorable, in the case of the electric field due to the locally weakened field, in the case of the diffusion flux because diffusion paths to the base are longer and are often obstructed by the already deposited structures. The spherical diffusion flux model by Monroe and Newman [54] additionally predicts that the growth of a needle accelerates with time. For our galvanostatic conditions, we found that needles continually decelerated and eventually seized to grow.

Up to now, the model of Yamaki et al. [62] of whisker-like growth has been the only one to explain the observed growth at the base of a needle. They were also the first ones to introduce the term “whisker” instead of dendrite, which is consistent with what we call needle-like growth. A classical dendrite in materials science or electrochemistry describes a fern- or snowflake-like structure [100] that is growing by deposition at the tip, whereas a classical whisker is typically a crystalline structure, often with a high aspect ratio. The mechanism of growth of many whiskers is still not clear but whiskers are considered to either grow from the tip or base. An observation like the one made here, where growth happens at the base, at the tip, as well as between two kinks is not in agreement with conventional whisker growth models. The model by Yamaki et al. where lithium whisker growth is described as a stress induced process similar to the growth of tin whiskers, can hardly explain the growth within a kinked filament as shown in **Fig. 5.4**, as this would require another extrusion process inside the whisker. This is unlikely due to the following: i) At the growing structure, the SEI should be thin. Therefore, the stress buildup which is supposed to be related to the confinement of the SEI film would be smaller than on the structures deposited earlier. ii) Within the whisker, there is no extrusion hole. iii) There is hardly a pressurized volume and only a limited surface area around kinks to supply enough lithium for this growth mechanism. From the observations performed here, it seems that the formation of lithium whiskers can occur without stresses or – more precisely – stress gradients that trigger the formation of tin whiskers.[101] It can be concluded that the extrusion model is not suitable to explain the filament growth for the electrolyte and rate used here. We suggest that the growth occurs by immediate addition of lattice planes to the existing whisker.

A consequence of this rather local insertion is that shorter diffusion paths inside the solid are required as compared to tin

whisker growth. During whisker growth, diffusion of tin atoms towards the whisker along grain boundaries over distances of several microns occurs. For the mechanism considered here (**Fig. 5.6**) the maximum distance is the diameter of the lithium filament. Another important process might be surface diffusion: For tin, lateral diffusion over enormous distances is possible;[102] similar to that, we consider surface diffusion of lithium atoms as a possible mechanism for the delivery of the atoms needed for growth.

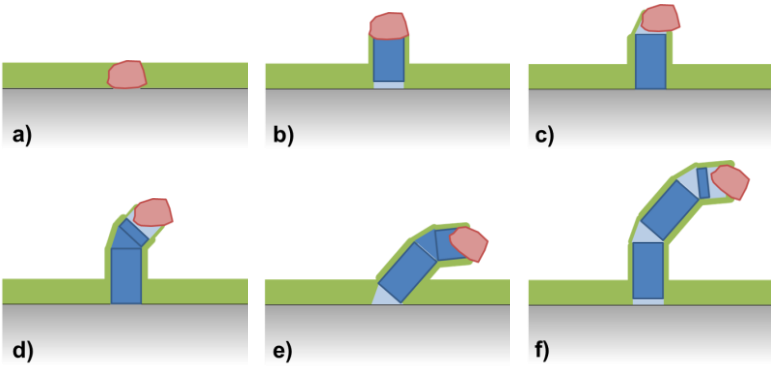

Fig. 5.6: Schematic describing growth of a lithium needle as observed in the *in situ* videos. The homogeneous components of the SEI – which are probably mainly organic – are drawn in green, Li insertion areas are light blue. The inoxidizable feature at the tip is depicted in red. a) initial state before lithium deposition with the inhomogeneity of the SEI shown in red, b) after growing a straight segment by lithium insertion at the substrate, c) after further deposition taking place below the tip, d) further deposition can result in a kink, e) additional Li was inserted at the base, causing tilting motions of the whole structure, f) final structure. All steps proceed by lithium insertion into the growing structure.

The whisker-like growth of the lithium filaments observed here with a growth at the base is quite different from the usual

dendritic growth which – by the definition of "dendrite" – includes branching. Typical dendrites often have a regular, quasi-periodic branching pattern, but irregular structures occur for the conditions where the diffusion limited aggregation model [99] applies. No regular branching has been observed by us or reported in the literature for lithium deposits, i.e. the known "lithium dendrites" are irregular, non-uniform structures.

It has already been reported that Li needles can grow at either the tip or the base in a imidazolium chloroaluminate electrolyte, for which needles are expected to be much larger than in conventional electrolytes.[103] In our case, we observed Li filament growth in the widely-spread EC/DMC/LiPF6 electrolyte, even though dendrites in EC:DMC have been told be too small to be imaged using a light microscope.[103] Our key observation is that lithium metal filaments do not grow exactly at the tip, but behind an inactive structure at the tip and that growth is also possible in between the base and the tip. Both processes require the insertion of metal atoms. This can happen at the substrate-lithium interface or at crystalline defects such as kinks since the insertion of atoms into the volume of an intact crystalline solid is unlikely from an energetic point of view. It may be possible that the efficiency of the defect for lithium insertion depends on the degree of crystalline disorder associated with the defect. In this context, large angle boundaries or amorphous regions could lead to fast insertion. Our growth hypothesis (**Fig. 5.6**) is based on ionic and atomic lithium diffusion and insertion and does not include the macroscopic process of plastic deformation and flow.[62]

In addition to this insertion of lithium into growing structures which are probably crystalline,[104] further details can be inferred from the observations. The structures at the tip (which we observed as extra features on some filaments in SEM images as the one shown in **Fig. 5.7**) which are not dissolved during ano-

dization (**Fig. 5.5**) may be inoxidizable particles that participate in filament nucleation as suggested in **Fig. 5.6** a)–b), e.g. by changing the local SEI resistance, and in the propagation as proposed in **Fig. 5.6** c)–d). On the other hand, the inoxidizable particle can be a cap of SEI that forms during lithium deposition.

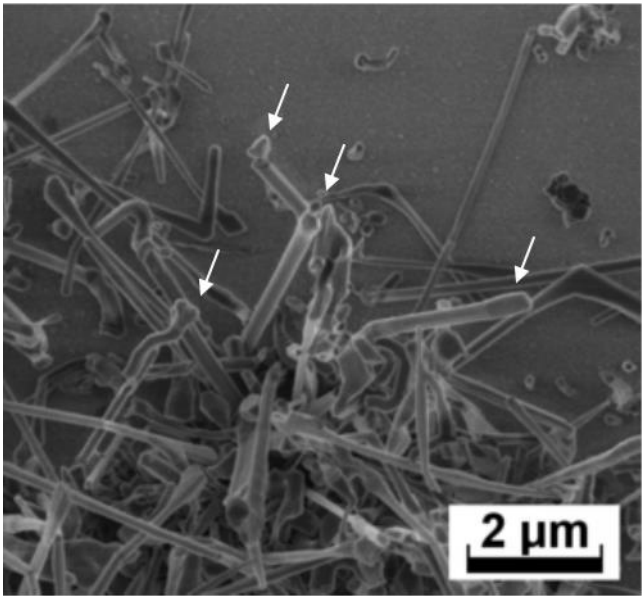

Fig. 5.7: SEM image (1 kV) of lithium filaments deposited on tungsten at −100 mV. Several filaments show structures at the tip e.g. contrast changes, contaminants such as particles or a broadening of the tip.

An ideal SEI would be completely homogeneous, causing homogeneous plating at its interface to the metal. However, an actual SEI will never be uniform and may include inorganic crystals of oxide, hydroxide, carbonate or fluoride or other components depending on the electrolyte composition.[105] Due to variations

in the local conductivity or preferred aggregation of the discharged lithium atoms at irregularities in the SEI – drawn in red in **Fig. 5.6**, the lithium metal structure can grow relatively fast at this localized defect, causing an instability with respect to uniform growth.

After nucleation, atoms can be added at defect locations, i.e. either the substrate/needle interface, at the top inorganic particle/lithium interface or at kinks along the needle. For this process, the permeability of the SEI is of importance. The freshly formed SEI which grows on the lithium filament has to be thin enough since a thick SEI would slow down metal deposition. If growth would be mainly controlled by the insertion at regions where the SEI is thin it would not be possible to explain the observed 1D growth, instead rounded shapes like Fig. A 2 should result. In addition to SEI regions that are thin enough also crystalline defects are required. It may be assumed that the SEI is modified at defects, e.g. the growing SEI is quickly carried away with the growing metal so that the SEI remains thin at the insertion site.

Kinks can either form by a change in growth direction at the tip as suggested in **Fig. 5.6** c–d, or at the base (**Fig. 5.6** d–f). We would like to emphasize that the growth zones of our model, placed in kinks or interfaces, easily explain the strong shaking and twisting motion that are present in the videos and that have been already observed by others [94, 106]. In [94], the swinging behavior was explained by residual stress, but the large amplitude and angles involved would again require strong plastic deformation. In the interface or defect dominated growth presented here no stresses are needed to explain the motion of the growing structures. Instead, the motion is a consequence of non-uniform insertion at the base or at kinks.

Finally we emphasize that our observations have been performed with a particular liquid electrolyte (LP30, i.e.

EC/DMC/$LiPF_6$) and a limited range of potentials and currents. For other cases, e.g. for higher currents or for polymer electrolytes with lower conductivity and lack of convection, the strong concentration gradient or even total depletion which are crucial for the models by Monroe and Newman [54] or Chazalviel et al. [19-21], respectively, can occur so that the corresponding models are applicable. The same is true for the other models: If there is growth at the tip, it will be faster due to spherical diffusion, but our observation of growth at the base suggests that this diffusion criterion alone is not sufficient to explain the strong tendency of lithium to form non-planar electrodeposits.

5.4 Conclusion

The growth and dissolution of electrodeposited lithium filaments have been observed. In addition to accretion at the tip region, unusual growth modes have been observed: growth in between kinks, but also growth from the base. Tip growth does not seem to occur at the outermost top, but behind an inactive structure. Based on the observations we suggest growth being dominated by insertion at crystalline defects, e.g. kinks or interfaces (**Fig. 5.6**). This should also apply similarly for so called bush-like or dendritic lithium. Several types of defects have to be considered: thin parts of the SEI causing enhanced deposition, defects in the crystal structure such as grain boundaries or maybe even amorphous regions, and chemical inhomogeneities such as contaminants that can cause alloy formation or may act as nucleation centers. For the conditions that we used during deposition, especially the liquid electrolyte, the observations are not compatible with previous explanations of lithium dendrite growth, e.g. with models that emphasize the field enhancement at tips, the strong influence of concentration gradients or the stress induced extrusion or motion.

6 Mechanisms of Bush Growth

The formation, growth and shrinkage of lithium bushes were monitored by *in situ* light microscopy and by *ex situ* SEM studies. This chapter was published in [2].

6.1 Results

Lithium was deposited and dissolved under galvanostatic conditions. The electrode and the lithium structures were observed *in situ* by light microscopy. **Fig. 6.1** and the corresponding video S 1 show the growth of a needle-like structure that is surrounded by a bush. Between images a) and c) this structure grew in a straight line and gained in length. Minor variations in the apparent diameter in the video images occur if the filament runs out of focus, but since a decrease of the diameter during electrodeposition is hardly possible, it is reasonable to assume that the diameter did not change at all. The tip seems unchanged during growth; therefore, growth at the tip is unlikely for this structure. The view on the exact growth zone however, is blocked by the surrounding bush. Starting from picture d), the structure started to grow in width at the tip where significant roughness is visible. From there on the straight needle part did not grow extensively anymore and instead the tip widened showing even more structure and curling indicative of, e.g., branching.

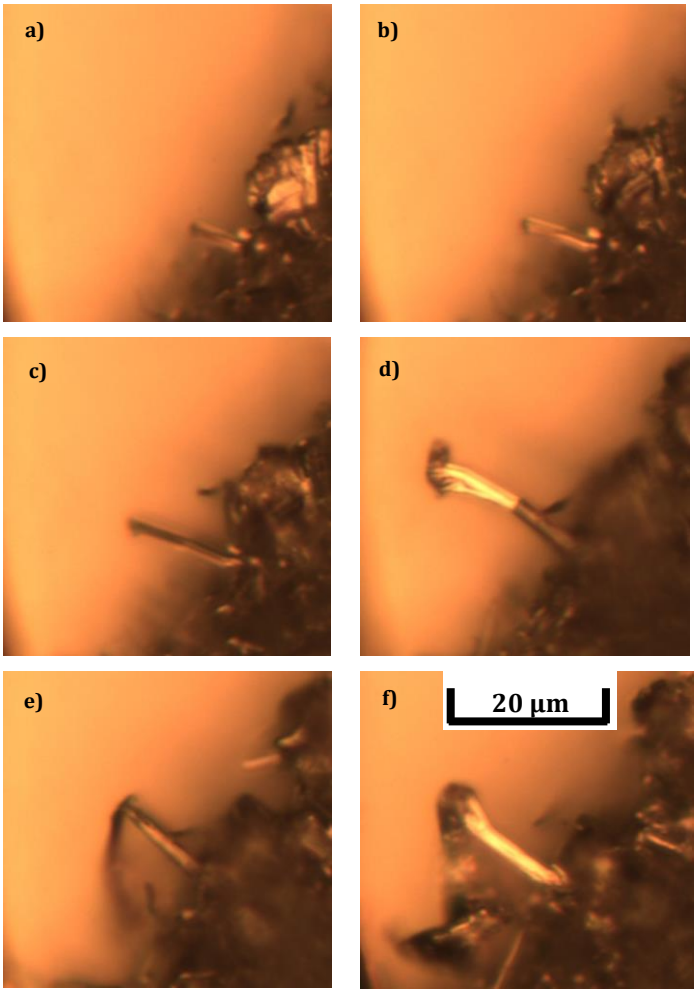

Fig. 6.1: *In situ* light microscopy of a structure during continuous **electrodeposition** on tungsten. First, it is needle-like and gets pushed out of a bush-like structure. At the beginning, the needle increases in length, then changes its growth behavior in picture d). It starts to increase in diameter, and later also curls. The images cover a time span of 30 minutes.

Fig. 6.2 and video S 2[4] show bush-like growth recorded by laser scanning microscopy; the structure is shown in side view, i.e. perpendicular to the line connecting working and counter electrode. The circles mark arbitrary, but easily traceable structures of the bush. The arrows in image b) mark their shift in position from their original position (image a)). These structures lack a preferred growth direction and they also increase the distance between each other.

To inspect bush structures, we used a micromanipulator (Kleindiek Nanotechnik) inside an SEM to remove the upper parts of a lithium bush, where we found needles underneath (see area marked in red in Fig. A 3). Furthermore, we used the FIB to image cross sections of Li bushes. An example is shown in **Fig. 6.3**. It can be seen that large parts of the structure are not directly connected to the substrate.

The dissolution of the bush-like structure depicted in **Fig. 6.1** is shown in Fig. A 4. The process started at the tip and was accompanied by the motion of the whole structure. The images suggest that the lithium of the broadened filament could be dissolved and only a thin shell of the structure remained. In contrast to this case where a large fraction of the metal could be redissolved, the case of an incomplete dissolution is shown **Fig. 6.4** (cf. the video S 5[4]): in image a), a bush structure is shown that was electrodeposited on copper, and image b) shows what remained of the structure after its dissolution up to 3 V vs. Li. The arrows mark a structure at the tip of the bush that did not change its shape while the bush was shrinking.

[4] The video can be found online in the supplementary info of [79].

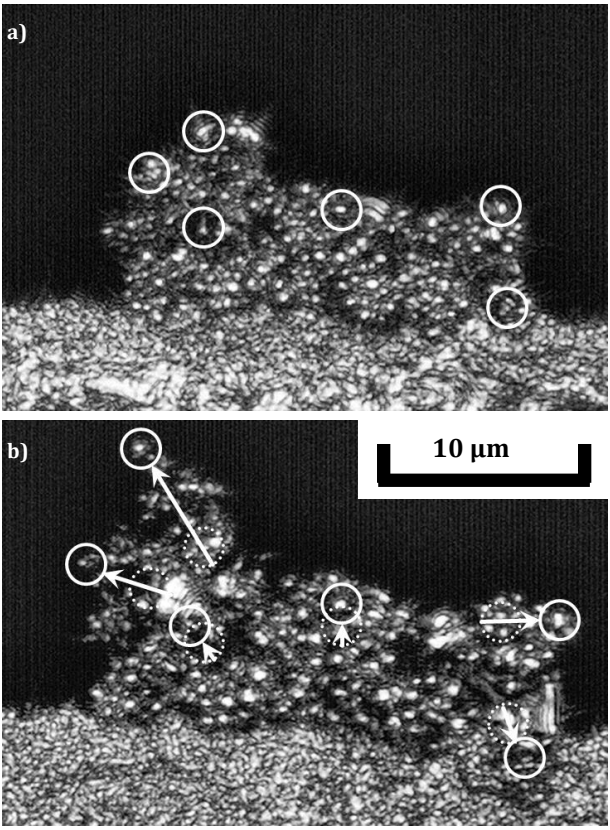

Fig. 6.2: *In situ* images – 45 minutes apart – of a Li bush growing on copper foil in LP30 electrolyte, in side view, during continuous electrodeposition. The circles mark traceable structures of the bush, and the arrows in b) mark the shift in distance from their original position in a). The counter electrode is located above the Li bush, outside the field of view.

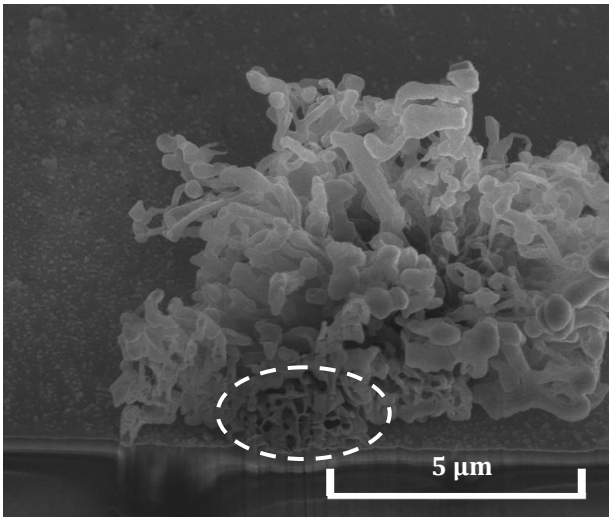

Fig. 6.3: SEM image (5 kV) of a FIB **cross section of a lithium bush** grown in LP30 electrolyte on a tungsten substrate on glass. The part of the bush that connects to the substrate is marked.

The two following images show a subsequent plating step. No new bushes have been observed; instead the electrodeposition took place at the location of the remaining bush. While the tip structure of the bush remained unchanged both during dissolution and deposition, the bush changed its size and seemed to grow towards the sides and around the inactive tip structure. Again, no obvious general growth direction was observed during electrodeposition. The fact that a large part of the structure of **Fig. 6.4** could not be dissolved is also reflected in the galvanostatic data (see **Fig. 5.1** for a representative graph) where it was apparent that the amount of charge transferred during stripping is significantly smaller than the amount of charge transferred during electrodeposition.

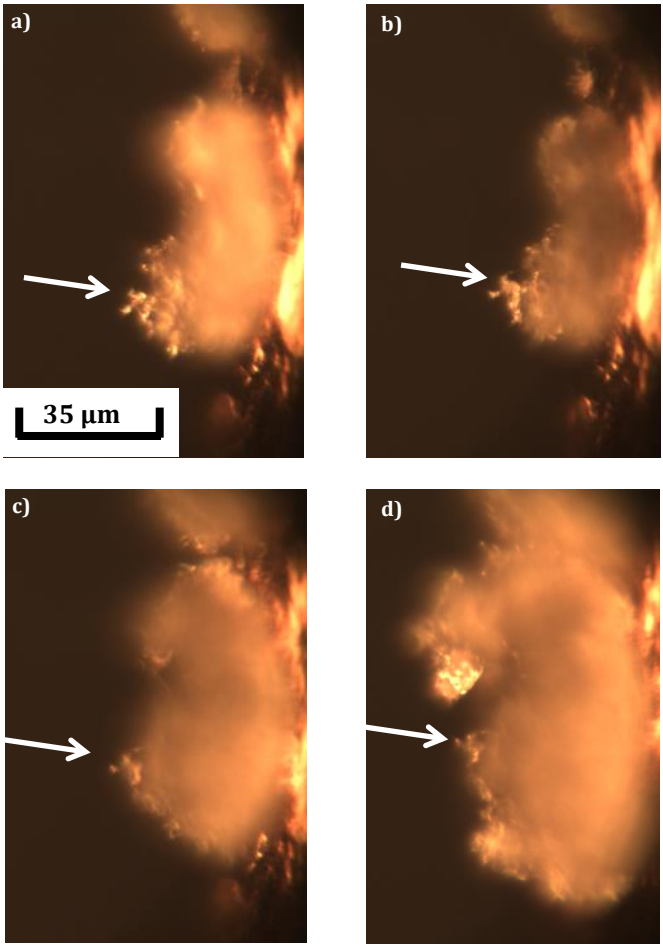

Fig. 6.4: *In situ* light microscopy of the dissolution of a bush on copper foil (between a) and b)) with subsequent continuous electrodeposition (b), c), and d)) in side view. The counter electrode is located on the left outside the field of view. The tip structure (marked by the arrow) remained unchanged during stripping and plating. There is no obvious general growth direction. The images cover a time span of 30 minutes.

Fig. A 5 shows an overview of a tungsten surface during growth showing lithium needles and particles. All structures on the substrate have nucleated at roughly the same time. The arrows mark lithium structures that formed and ceased to grow, while other structures continued to grow. Although Fig. A 5 only shows this effect for bush-like growth, we also observed this effect in needle-like growth. These active structures also remained active after interrupting deposition for one hour for several times.

6.2 Discussion

6.2.1 Growth of Li Bushes

The observations as exemplified by **Fig. 6.1** clearly demonstrate that growth can happen both at the tip and at lower parts simultaneously. The tip broadening (**Fig. 6.1** d)) proves accretion at the tip; at the same time, the features of the filament tilt and move outwards showing that the base is flexible and still growing. Based on our observations of single Li needles we suggest that lithium is inserted either at the tip, the base or at kinks of whisker-like structures, and we conclude that defects are necessary to allow lithium atom insertion into a filament. In particular, insertion into intact crystal structures is unlikely; therefore, we believe that defects for example such as grain boundaries are required to allow Li atom insertion in the otherwise perfect crystals. Kinks in filaments with straight segments were observed frequently in our microscopic images. They are an experimental indication of high angle grain boundaries which are regions of high defect density containing dislocations and/or vacancies. The tilting movements indicate that these grain boundaries do not have fixed angles, which suggests that their structure is either continuously chang-

ing by further Li addition or that it might have a liquid-like flexibility.

During lithium deposition, needle-like growth in length was observed frequently, which occurs – within the accuracy of light microscopy – without an increase in thickness. It has been described by the mechanism of insertion at kinks or other defects. Video S 1[5] and **Fig. 6.1** show that there is a transition between such needle-like growth, which is a quasi one-dimensional, linear elongation, and bush-like growth, which is three-dimensional and includes branching and the multiplication of defects. The growth in images a) to c) was clearly a one-dimensional needle elongation with a growth zone outside the field of view. In images d) to f), additional growth occurred inside the field of view, and was three-dimensional with no discrete atom insertion point. That is why it is suspected that there are mechanisms for the multiplication of defects (and hence, lithium insertion points) so that branched structures can form starting from a needle. So far both growth modes have been treated separately. The growth of 3D structures may bear resemblance to the growth of needles, but with the further requirement that the simultaneous insertion at additional locations has to take place. For example the particle on the right in video S 1[6] expands in a way that suggests that this growth does not happen by attachment at its perimeter only. It appears to be polycrystalline and seems to consist of crystallites that have straight edges. For this case growth may be mediated by simultaneous lithium insertion into different grain boundaries. Another possible explanation of this observation is that the particles are not fully metallic, but have deep grooves that contain SEI, which would explain the strong contrast between the crystallites. In such regions alleviated lithium insertion may be possible leading to 3D growth.

[5] The video can be found online in the supplementary info of [79].

In contrast to the suggestion of Yamaki et al. [62] based on observations in $LiAsF_6$ electrolyte, the insertion of lithium does not necessarily happen at the base, which is at the substrate/lithium interface in our case. Instead, the growth occurs by lithium insertion into different growth regions which can be distant from the current collector. The growth of lithium dendrites occurring either at the tip or "at the base" was observed by Crowther and West [25] as well. Close inspection of their results shows that even in their case the growth might not be limited to these two insertion sites and growth similar to our observations may be inferred from their video. It is not likely that the growth at the substrate/lithium interface is an effect of a particular substrate metal, because Crowther and West used a copper electrode [25], Yamaki shows an SEM image of lithium on a stainless steel substrate [62], and we used tungsten films and copper foil substrates. Therefore, we think that the Li growth mode with an insertion at the lithium-substrate interface or close to it might not depend strongly on the substrate material, but is rather a property of the lithium metal itself.

The growth of lithium bushes shown in **Fig. 6.1** and **Fig. 6.2** resembles the raisin bread expansion model (known as a cosmological model [107]). In this model, there is no preferred direction and the distance between every raisin in the bread increases as the bread expands. However, in the case of lithium moss, the videos show a strong random component superimposed to the overall expansion. This is due to the statistical nature of several processes. These are: nucleation events, growth speed, the distribution of growth directions as well as the kinking that causes bending of dendrites and sudden movements. Sometimes large dendrite parts fold in by a pronounced rotation. Therefore, the growth occurring on top and in between rigid metallic structures is less uniform as the simple raisin bread model might suggest. The growth of the raisin bread has no growth center, but the

movement of its parts can be restricted due to the support of it. In our case of Li, the metal substrate fixes the bases of the bushes. In the case of the lithium bush, lithium atoms are inserted into the bush at several points that are scattered over the whole structure. Certainly, this "raisin bread" model – which is illustrated in **Fig. 6.5** by the transition from a) to b) – is hardly dependent of the substrate morphology or material since it describes processes occurring within the bush-like metallic lithium structure.

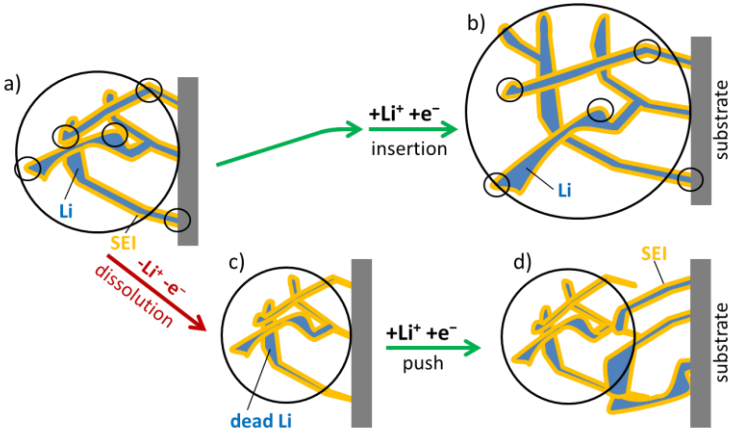

Fig. 6.5: Schematic of suggested growth of moss structures. The structure is always covered by a SEI layer. a) as deposited, b) the structure of a) after further electrodeposition. Li atoms are inserted into the metal structure. Points (to be compared with raisins in rising dough) have been marked with black circles to illustrate that the distances between these features generally increase with Li deposition time. The large black oval shape indicates the expansion of the total structure. c) the structure of a) after a dissolution step. The tips of the structure still contain Li metal ("dead lithium") but are electrically isolated from the substrate, although still being held by the former SEI shell, d) structure of c) after an additional electrodeposition step. The top is pushed outward by the new lithium moss growing underneath.

A very dynamic behavior of lithium, especially rotation [108] and swinging [94, 106] of filaments has been reported before. It has been explained by stresses, in particular due to a non-uniform distribution of mechanical properties of the SEI [106]. Based on our observations, we suggest an alternative explanation: Movements might arise without stresses or external forces acting on the metal by non-uniform insertion. If the Li incorporation or crystallization is faster at one side, the inserted Li will have a wedge profile instead of the plane-parallel layers which are required for elongation without tilting. The inclination of the wedge might change with time if more Li is added, causing tilting or swinging motion of the whole upper part of the filament or dendrite. The forces involved here are negligible, especially compared to the forces of plastic deformation of the metallic core that has been assumed before [62, 106].

Based on TEM observations using ionic liquids, it was suggested that Li filaments grow parallel to the electric field [109], and that field enhancement directs the growth [104]. In our opinion, the observed movements together with the randomness of growth suggest that the direction of the growth does not depend on the electrostatic fields in our LiPF6 electrolyte solution. In spite of the observed omnidirectional growth of large bushes, indications were found that there can be a transition from linear to omnidirectional growth. In the cross section of **Fig. 6.3**, practically all filaments are distant from the substrate. However, a small part in the lower middle of the image (marked) seems to be connected to the substrate; this is probably the region where the growth of the bush was initiated (its “stem”). This stem has a quite complex structure of very fine filaments; some of them with diameters well below 0.1 µm, whereas the structures above the stem can have diameters of more than 0.5 µm. Thin lithium stems in the moss

have been already suggested by Arakawa et al. in their Fig. 2 [110] pointing towards a growth mode transition during moss growth. **Fig. 6.3** further supports the argument of this transition, as it shows that thin needles formed the base on which the more bulky lithium plated afterwards. Again defects seem to be responsible for the formation and transition. Once defects (insertion sites) can multiply and become simultaneously active, needles can transition towards bushes. Our observations indicate that whisker-like needles can grow to broader structures that may branch without the need of a pronounced step of nucleating a fresh particle on the existing whisker.

The growth modes that we observed in $LiPF_6$ electrolyte do not resemble the most typical dendritic growth with almost regular branching. According to the data presented here the term "lithium dendrite" describes quite randomly branched structures as exemplified by diffusion-limited aggregate (DLA) models [99, 111]. However, several aspects distinguish our suggested growth mode from DLA: Our "dendritic growth" includes the insertion of lithium into the backbone of the existing and growing branched structure. The branching that we describe happens by broadening and forking during growth whereas branching in DLA always requires a nucleation step (that can happen at random time long after the formation of the underlying structure) similar to the nucleation of a filament on the substrate.

6.2.2 Dissolution of Li and Insulation of Li

If a bush with "thin stems" (**Fig. 6.3**) is dissolved, it is easy to imagine that the lithium of the fine stem structures is consumed before that of the branches if we assume that the dissolution proceeds simultaneously on all Li surfaces. If the lithium of a single needle is dissolved, residues of SEI remain as an empty shell. Accordingly, a SEI-like residue will remain if the lithium is

removed from the inner part of the stems (**Fig. 6.5** a) to c)), keeping the rest of the moss attached to the surface (**Fig. 6.5** c)). Lithium of the more massive upper filaments persists since the dissolution caused electrical insulation from the substrate. This remaining lithium is "dead lithium" since it is electrochemically inactive during further cycling, although it stays chemically active .[112] It can be a major part of the capacity loss in Li electrodes.[72] In addition to dead lithium, repeated formation of SEI shells on new dendrites will cause degradation by repeated electrolyte decomposition. The total loss of capacity can also be seen in galvanostatic curves, which in our case typically showed that about 30 % of the deposited lithium could not be dissolved **Fig. 5.1**.

Insulated lithium has been reported earlier.[112, 113] Peled suggested that it is a Li ball embedded in the SEI layer.[113] The name "dead lithium" was coined by Yoshimatsu et al. [114]; they emphasized the role of dendritic growth followed by dissolution which causes insulation. In contrast to the illustration in [114] where the lithium is detaching from the electrode and falling apart during dissolution, we suggest that the structure can keep – at least partially – its mechanical integrity, as the SEI shell of the already dissolved metal remains attached to the substrate and to other lithium structures. Our interpretation combines aspects of previous results – dead Li can remain firmly attached to the substrate [112] while it is covered with SEI similar to the embedded Li suggested by Peled [113]. The 3D dendritic growth itself makes the lithium susceptible to insulation as described in [114]. We add the new aspect of a ramified structure held together by a continuous SEI shell. In addition, the highly kinked and crooked active and dead lithium metal might be mechanically intertwined in the dense bushes, resulting in structural stability. According to these arguments, active and dead lithium regions are then a result of the properties and thickness of separating SEI regions.

6.2.3 Electrodeposition After Dissolution – "Push Remnant" Mechanism

Fig. 6.5 shows the most probable scenario to explain the observations in **Fig. 6.4**. During redeposition (the steps from **Fig. 6.4** c) to d)), deposition at the tips of the old mossy structure is not possible; therefore, deposition must again occur at lower places – in our case, at the substrate – since all lithium electrically connected to the substrate has been dissolved. The freshly growing lithium pushes the remnants of the old moss away (from **Fig. 6.4** c) to d)), and later freshly growing tips will outdistance the old ones. The schematic in **Fig. 6.5** is based on many observations like the one shown in **Fig. 6.4**. **Fig. 6.5** shows the two types of growth in comparison. The growth where dead lithium is pushed away (**Fig. 6.4** b) to d)) has to be clearly separated from the non-tip growth of active lithium (exemplified by **Fig. 6.2**) discussed before. Both growth modes look very similar in the microscopic images which do not show a visible difference between dead and active moss if it contains metallic Li. For both growth modes, the Li attachment does not occur at the tips, as expected according to usual dendritic growth models. Insertion into active structures was previously described as insertion at the base by Yamaki et al. [62] and by Crowther and West [25]. The insertion below insulated moss is a process not yet discussed in the literature that obviously excludes that the advancement happens at the outermost visible tips. Even in cases without dissolution the "push remnant Li" mechanism might be relevant: If the electrodeposition results in very fine stems of a bush, one can imagine that the formation of a thick SEI layer on them can consume their Li and cause insulation of the top structures.

6.2.4 Factors Affecting Nucleation and Dendritic Growth

Deposition below the remaining SEI structure is preferred over the nucleation of new structures. This is surprising since remnants obstruct Li^+ diffusion between the electrodes: The diffusion path necessary for direct plating at a flat interface is shorter and more accessible than the longer and obstructed path for the electrodeposition below the remnants of a bush. This makes this path unfavorable, and mechanisms based on ionic depletion in the electrolyte cannot account for this observation. This means that depletion of Li^+ ions near the electrode surface is not needed for the initiation of dendritic growth of Li. This conclusion has been made before based on the high Li concentration at the substrate surface at dendrite initiation [108]. Here it is assumed that the diffusion in the electrolyte is obstructed by the remnants causing decreased conductivity. However, the opposite might be the case: solid particles can enhance the conductivity of electrolytes by ionic adsorption ("soggy sand" electrolytes [115-117]). If the remnant parts acted as "soggy sand" causing enhanced Li^+ transport, the nucleation below the remnant would be a result of this increased ionic transport. Although this concept seems to offer an explanation of the unexpected result of deposition at sites that seems obstructed at first glance, it is speculative and is not used in the following. Other factors can be involved besides kinetic arguments such as diffusion kinetics: energetic reasons might lead to the insertion at a defect underneath the remnants. For example, the lithium insertion at a certain crystalline defect may require less energy than nucleation in a defect-free area with the associated nucleation overpotential.

The observation that some needles and bushes seize to grow during deposition as shown in Fig. A 5 can be interpreted as a growth competition between the structures. A possible explana-

tion may be that larger and faster-growing structures localize the deposition in a certain area around them. This would cause neighboring structures to stop growing as the process becomes diffusion limited and the electrolyte depletes of lithium ions around an active structure. However, this point becomes questionable when looking at the two large structures in the lower part of the images in Fig. A 5. These two structures did not seize to grow, and their growth speed did not seem to slow down even when they further approach until they touched. The fast growth of these adjacent features in Fig. A 5 combined with a slowdown on the same electrode suggests that the growth rate is not diffusion-limited. This interpretation deviates from previous conclusions: For PC electrolytes, plotting the length of bush structures vs. the square root $\sqrt{t}$ of time gave a linear graph. This has been explained by diffusion control.[108] Irrespective of such concentration gradients, galvanostatic conditions force deposition at constant rate. Depending on the geometry, different scaling with time will result. A $\sqrt[3]{t}$ dependence would result if one could assume that the bushes have a constant mean density and grow isotropically. In our experiments, the growth direction seems to change randomly. If the direction of growth of a tip changed from time to time into a random direction, the random walk model would be applicable, and the distance travelled would also follow a $\sqrt{t}$ relation.

The insertion mechanism suggested here is based on defects in the crystal structure and in the SEI. Some defects are short-lived for lithium: Its low melting point (454 K, i.e. for our experiments done at room temperature $T \approx 0.65\ T_m$) and the recrystallization temperature for partially transformed lithium (200 to 230 K, i.e. $\approx 0.5\ T_m$) [118] argue for a considerable lithium atom mobility and fast recrystallization. Therefore, even during a fast deposition, the number of defects such as dislocations remains limited. High angle grain boundaries – which can be associated with kinks that are visible in the microscopic images – and the substrate/lithium

interface are probably the most relevant crystallographic defects. Defects in the SEI, for example thin parts or even cracks, occur as a consequence of lithium growth and the corresponding increase in surface area. Major defects in the SEI are also short-lived since Li is very reactive, causing a fast (≤ 1 s) formation of an initial SEI [119].

The observations show that after growth interrupts for one hour, the growth continues in the same way as before the interrupts, i.e. the bushes that are active stay active and the inactive ones remain inactive. During the interrupt there should be sufficient time for the healing of short-lived defects so that these may be excluded from being responsible for the selection of preferred bushes. Such mechanisms include crystalline defects in the lithium like dislocations and grain boundaries and interface effects in the SEI. Here thinned regions with low impedance might locally accelerate growth but would heal within the mentioned time scale. Since short-lived defects can be excluded, self enhancing growth can also be excluded as a dominant mechanism. In such a process, preferred deposition through a thin SEI region would keep the SEI layer thin, thereby defining a growth region with a low resistance SEI. From the interrupted deposition it may be concluded that the growth mechanism seems to be dominated by long-lived insertion sites or defects. Good candidates for these objects are kinks as well as the substrate interface. In the observations (cf. Fig. A 5) it can be seen that during growth, some of the bushes completely cease to grow indicating that the growth governing long-lived defects become deactivated. Although the dominant growth mechanism does not change after the growth interruption for one hour, during growth, the growth sites can change and the rather stable defects or insertion sites may become blocked.

6.3 Conclusions

Mossy growth of metallic battery anodes has to be avoided to minimize interface area and reduce electrolyte decomposition in cells. The growth and dissolution of lithium mossy structures is a very dynamic process involving non-linear, apparent random growth and motion of the tips of the lithium filaments which are not dominated by the direction of the electric field in the bulk electrolyte solution. During dissolution, large parts of the moss can get isolated from the current collector causing a loss of active material, known as “dead lithium” in the literature. Our results demonstrate that this can happen even if the material remains attached to its original position at the substrate. This attachment on the one hand and the observed motion and growth from below on the other hand increase the probability that metal that has been isolated from the current collector may get reconnected during charging.

Growth at the tips of lithium was observed, including the case of tip broadening. However, it was observed that mossy growth does not necessarily occur at the tips. Instead, the mossy growth often happens in growth points distributed throughout the moss. We suggest that grain boundaries, e.g. at kinks of needles or in between lithium particles, are the relevant growth points where lithium is inserted into the intact metallic backbone of the moss. Electric fields are not expected to have a large impact on this type of growth. Our results, e.g. the broadening of the filament shown in **Fig. 6.1**, give support to the view that lithium filaments are precursors of the mossy or “dendritic” lithium. Essential components of moss formation and growth are the insertion of lithium into defects sites as observed for needles, the branching of lithium structures and the simultaneous activity of several insertion sites. The transition from filaments (1D) to moss (3D) growth occurs by broadening and branching during filament growth. The corre-

sponding mechanism is neither a regular branching based on periodic instabilities as for dendrites with a regular forking pattern causing a fern-like appearance, nor a later branch nucleation step on an preexisting structure at a random time as suggested by the diffusion limited aggregation model. Instead, the observed branching started with a continuously increasing tip width. We suggest a growth mechanism involving the multiplication of crystalline defects.

7 The effect of Crystalline Orientation of the Substrate

It was shown that the electrochemical formation of copper dendrites grown by diffusion limitation is not only controlled by transport phenomena but also by interfacial processes.[120, 121] Copper dendrites were grown on copper single crystals with different orientations and a dependence of the kinetic overpotential on the crystal orientation was observed when 2 mM of chloride was added to the acid sulfate electrolyte. Without the chloride, this dependency was absent. We also studied the influence of interfacial processes on the electrochemical deposition behavior of lithium. We chose polycrystalline copper substrates and mapped the orientation of the grains by EBSD. This technique allows for the simultaneous investigation and comparison of multiple orientations in contrast to conventional electrochemical experiments on individual single crystals.

Vibratory polished and oxide free copper samples with hat shape ("hat samples") were annealed; lithium was deposited potentiostatically using the hanging meniscus technique in the *ex situ* beaker cell. The samples were then transferred into the SEM for imaging. After the SEM images were taken, the samples were rinsed with deionized water to dissolve the lithium, dried and again transferred into the SEM. Here, orientation maps of the copper substrate were recorded by EBSD measurements.

7.1 Results

The images of **Fig. 7.1** a) and b) show SEM images the resulting deposits for LP30 (-100 mV for 60 s) and a 1 M LiTFSI in DOL (-100 mV for 30 s) electrolyte respectively. The deposition was

inhomogeneously distributed over the sample surface, while small areas with a homogeneous distribution of deposits were observed. Depending on the detector, dark or bright color represents areas that are more or less densely populated by lithium needles and particles (as shown in **Fig. 7.1**). With an SE2 detector, densely populated areas appear dark; with an "in lens" detector those areas appear bright. **Fig. 7.2** a) and **Fig. 7.3** a) show an overview over the sample surface after lithium deposition in LP30 and the LiTFSI electrolyte respectively, together with an out-of-plane orientation map of the same areas after washing. The orientation maps showed that the homogeneously populated areas correspond to grains of the copper substrate. It also shows that the most densely populated grains had {111} planes parallel to the sample surface (blue grains in the orientation map) in both electrolytes. With increasing deviation from this orientation, the grains showed less lithium.

7.2 Discussion

Langhuizen [93] also observed an inhomogeneous distribution of deposited lithium with small homogenously populated areas on a nickel substrate in a 1 M $LiPF_6$ in EC:DEC electrolyte. However, he could only speculate about a possible influence of the substrate grains.

The fact that the grain orientation dependence was present in the two different electrolytes suggests that changing properties of the SEI (different electrolytes result in different SEIs) does not affect this dependency. To further elucidate the possible influence of the SEI, additional deposition experiments were conducted galvanostatically. During galvanostatic deposition, the potential gradually decreases, which means that the reduction potential of the electrolyte is reached before the reduction potential of Li. As a result, the SEI forms before lithium is deposited and lithium is

plated underneath the SEI. To further strengthen the SEI before the lithium is deposited, the SEI was generated by holding the applied potential at 50 mV vs. Li – i.e. just above the reduction potential of lithium ions – for two hours. The resulting deposits after applying 1 mA for 60 s still showed the same orientation dependency.

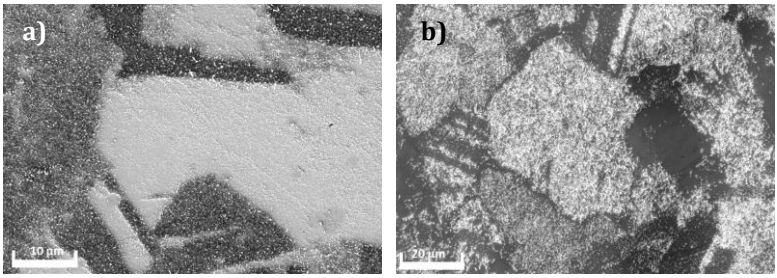

Fig. 7.1: (a) SEM image of lithium electrodeposited in LP30 on copper taken with the SE2 detector; densely populated areas appear dark. (b) SEM image of deposition in 1M LiTFSI in DOL taken with the "in lens" detector; densely populated areas appear bright.

During potentiostatic deposition the influence of the SEI is minimized, while it maximized for galvanostatic deposition combined with the preforming of the SEI. Under both conditions, the same substrate orientation dependence was found. This – plus the fact that we obtained the same results for a different electrolyte – suggests that this effect is not depending on the properties of the SEI, i.e. that it might be a purely crystalline interface effect. Possible is, for example, a low interface energy between lithium and {111} oriented copper planes. It could also be speculated about a connection between the (111) growth direction of needles and the preferred deposition on {111} oriented grains. Further investigation is needed to determine the influence of kinetics (e.g. Li adatom mobility on different grain orientations) and energetics (e.g. interface energy between lithium and copper).

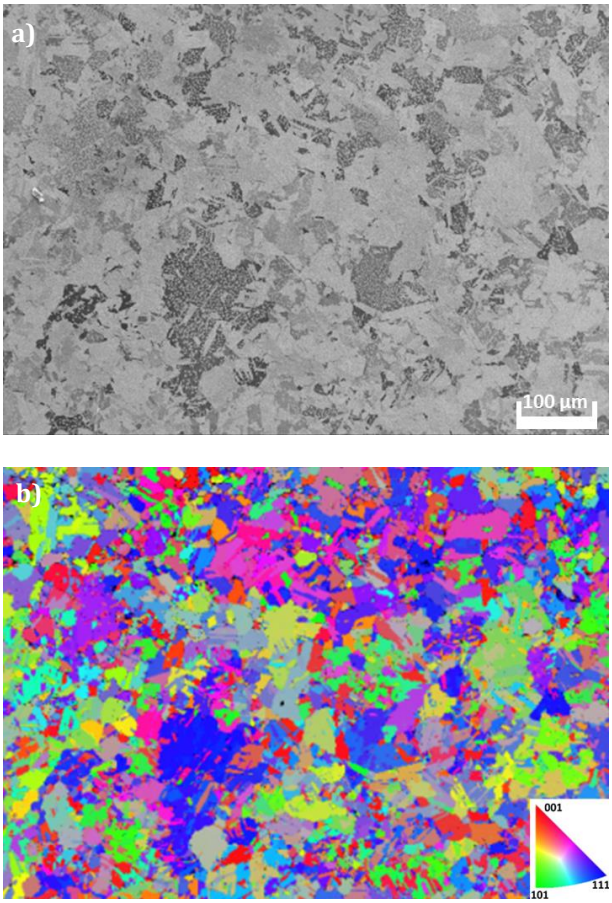

Fig. 7.2: (a) SEM image of lithium electrodeposited in LP30 onto copper. Image taken with the SE2 detector (i.e. densely populated areas are darker). (b) Orientation map (**in out of plane coloring**) of the same area of the copper substrate obtained by EBSD. {111} copper grains (blue) show the highest amount of electrodeposited lithium.

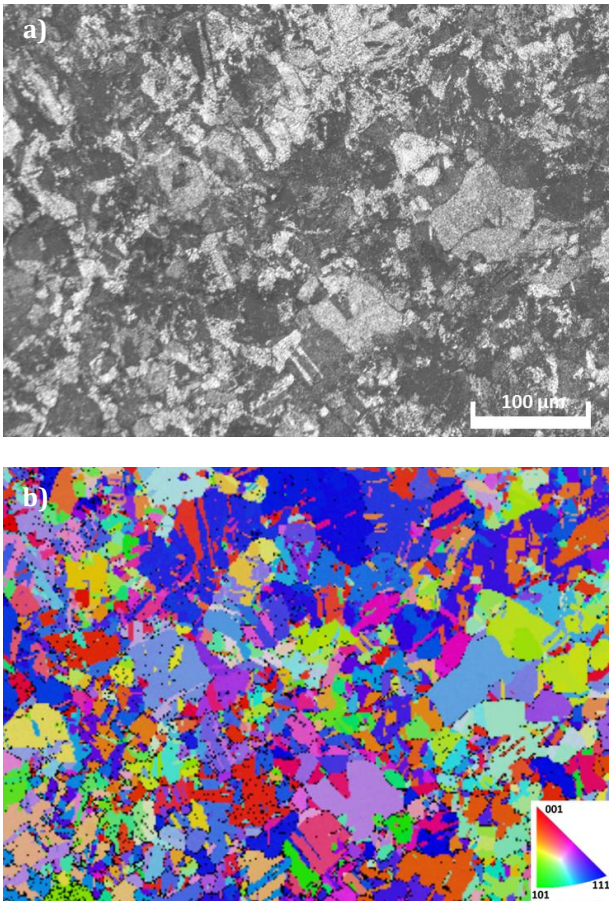

Fig. 7.3: (a) SEM image of lithium electrodeposited in 1 M LiTFSI in DOL onto copper. Image taken with the "in lens" detector (i.e. densely populated areas are brighter). (b) Orientation map (in out of plane coloring) of the same area of the copper substrate obtained by EBSD. {111} copper grains (blue) show the highest amount of electrodeposited lithium.

8 Lithium Whisker Growth Without Electrochemistry

So far it has not been clarified to what extend electrochemistry is involved in lithium dendrite growth. In order to elucidate this, experiments were performed to compare electrodeposition with physical vapor deposition of lithium. To investigate the mechanisms of filament growth and to what extent they are affected by the chemical composition of the electrolyte, we additionally compared dendrite formation in two chemically very different electrolytes, the widespread LP30 (1 M $LiPF_6$ in EC/DMC) and a 1 M LiTFSI solution in DOL/DME using the *in situ* light microscopy cell. The following chapter is in the progress of publishing [3].

In both electrolytes lithium exhibits the tendency to grow needles and dendrites. As observed before, lithium filament growth can occur by insertion at kinks (shown in **Fig. 8.1**), at the substrate interface and by growth at the tip (supplementary Fig. A 7 and Fig. A 8). The electrolytes have comparable ionic conductivities (11 mS cm^{-1} for LP30 [122] and 15 mS cm^{-1} for LiTFSI [32]) which implies that morphological differences are related to the different SEI compositions. Characteristic differences in the growth morphology were identified: First, in contrast to LP30, the TFSI based electrolyte shows spheres distributed along the filaments (marked by arrows in Fig. 1). Second, in LP30, needles can be elongated by insertion at the tip. In LiTFSI, the only growth observed at the tip was the deposition of lithium spheres in the tip area. Besides filament growth, also bushes or mossy lithium can form (**Fig. 8.2**). Here, strong differences were found: While LP30 shows strongly branched bushes where the branches resemble the filaments, electrodeposition in the LiTFSI exclusively leads to more compact agglomerates containing spheres. **Fig. 8.2** B is an

extreme example of such a structure not showing any elongated segments (as the ones shown in the lower part of **Fig. 8.1**) between spheres.

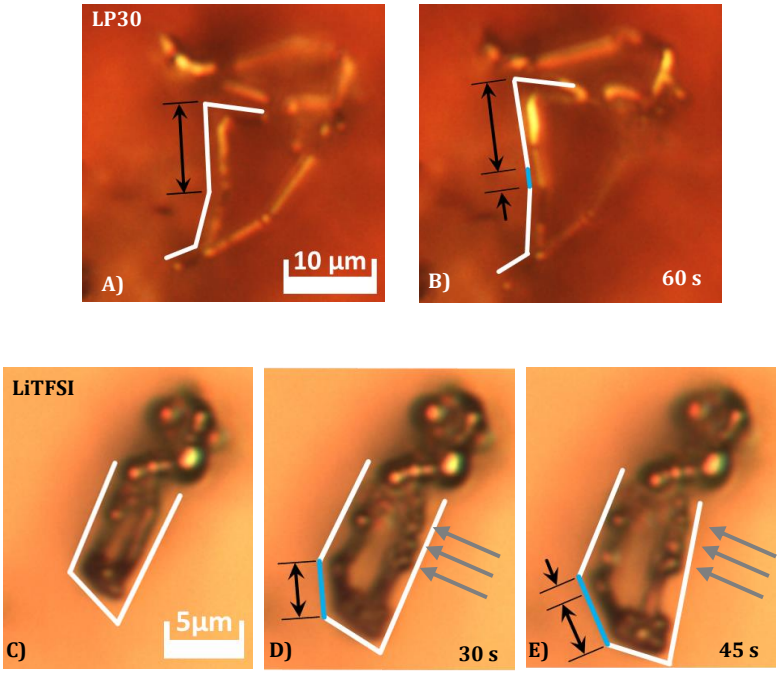

Fig. 8.1: Image sequences of the growth of a lithium filament in the shape of a loop (marked with parallel white lines) in LP30 (above) and LiTFSI (below). Both filaments elongate by addition of new segments (marked in blue) without elongation of the surrounding segments (white). Hence, the segments must grow by atom insertion into the lattice of the filament, probably at kinks. The arrows mark spheres that were plated at the side of a filament in LiTFSI. Image B) was taken 60 seconds after A). Image D) was taken 30 seconds and E) 45 seconds after C).

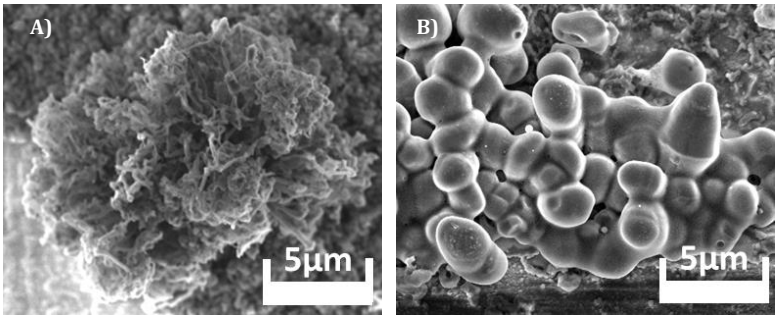

Fig. 8.2: SEM images of bush-like structures electrochemically grown on tungsten substrates. The bush in image A) was grown in LP30, the bush in B) in LiTFSI.

These differences indicate that the SEI has a strong influence on the growth morphology as reported before.[123, 124] The process of needle growth which is found for both electrolytes therefore does not necessarily depend on the composition of the SEI. To fully exclude electrochemical effects from the deposition process, namely electric fields, concentration gradients and the SEI, deposition was additionally performed by thermal evaporation (physical vapor deposition, PVD). **Fig. 8.3** shows SEM images of lithium needles on Cu grown by PVD in comparison with those obtained by electrodeposition. For the case of the electrochemical experiment, a SEI is present on the Cu surface. Nevertheless, the deposits look very similar: Both contain lithium needles with a length in the micrometer range and a diameter of ca. 0.1-0.2 µm. PVD filaments – which we observed in all PVD runs on different substrates – can have kinks as the electrodeposited ones (see Fig. A 8).

The strong resemblance of PVD and electrodeposited filaments (**Fig. 8.3** and Fig. A 9) indicates that the underlying mechanism

could be controlled by the same insertion mechanism.[6] As a consequence, electrochemical needle growth would not only be independent of SEI composition as suggested by the comparison of the two electrolytes above, but would not require a SEI at all. Accordingly, the tendency to form needle-like deposits would be an inherent property of metallic lithium. In this context lithium is no exception from other materials that form whiskers: In the field of vapor deposition the growth of whiskers, e.g. of copper or silicon, is a well-known phenomenon; it can be a useful fabrication route for nanostructures.[82] It occurs when deposition takes place at substrate temperatures above 65 % of the melting point of the deposited material.[6] Nanoscale whiskers have been observed for many metallic and a few inorganic materials on amorphous substrates.[82] This phenomenon is not well understood but experimental evidence [6, 82] supports the following description: During PVD, atoms are "raining" down homogenously onto the substrate which should result in an even, homogeneous layer. Hence, any protrusion in the resulting layer must be a result of the mobility and the rearrangement of adatoms on the substrate. On the substrate, the wetting properties vary, and a sufficiently high mobility of adatoms leads to the formation of agglomerates in the regions of the lowest interface energy. Due to the elevated temperatures and the associated high mobilities, crystalline configurations with low energies will develop. These small crystallites adopt the form of a Wulff construction [125] with the important difference that they additionally exhibit an interface with the substrate at a location where the wetting is favored. The non-wetting regions in the vicinity of the crystallites supply further atoms for the growth. The interface of the crystallite with the substrate is assumed to be the defect where adatoms are

[6] The deposits from PVD also showed what appears to be a grain orientation dependency, where certain grains were more densely populated than others Fig. A 6. This also points towards an insertion mechanism controlling both deposition techniques. However, we were not able to determine yet if the deposition is also preferred on {111} oriented grains.

continuously inserted and the facetted crystal is pushed forward to form an elongated whisker. For most materials, surface treatments (e.g. a carbon coating [6]) are needed to adjust the wetting properties to obtain whisker growth, however, in the case of lithium we observe this phenomenon without a pretreatment. The formation of needles in the PVD process as described here is based on the one hand on the fact that adatoms are highly mobile and consequently low energy configurations can develop and on the other hand persisting defects that allow for enhanced insertion. The similarity in the morphologies in **Fig. 8.3** suggests that these arguments may also apply for the electrochemical deposition.

An explanation suggested for the electrolytic growth of whiskers is based on the blocking effect of strongly absorbing components of the electrolyte (e.g. impurities) which can prevent the growth of certain crystal faces.[126] We have shown here that lithium filament growth by PVD and in the electrolyte is very similar, not only with respect to the morphology apparent in the images, but also with respect to the growth mechanism by insertion. The absence of the SEI in vacuum demonstrates that a mechanism based on blocking by the firmly attached SEI layer is not required to explain the propensity of lithium for filament formation.

Needle growth in PVD can only be explained by considerable adatom mobility. This might also be transferable to needle growth in electrodeposition. In our previous publications [1, 2], we showed that mechanisms like concentration gradients, spherical diffusion, SEI cracking or electric fields can been ruled out as the cause for the needle growth. However, if these effects have only a minor impact, there is no explanation for the inhomogeneous deposition as there is no mechanism directing the lithium ions in the electrolyte towards the insertion sites. Hence, it seems plausi-

ble that in electrodeposition, adatoms are first adsorbed at the entire electrode surface but remain mobile. Defect sites then act as sinks which form the initial needles. A high mobility of lithium adatoms is plausible due to the low melting point of lithium (T_m = 180.5 °C, i.e. RT ≈ 65 % T_m). The suggested adatom mobility mechanism also challenges the existence of the usual critical current density which needs to be exceeded to trigger dendritic growth [16, 127] and which is related to the ionic transport in solution [127].

Although we observed kinked, needle-like deposits during PVD of lithium, we did not find any bush-like deposits. This strongly suggests that bush growth is a phenomenon associated with the electrodeposition process. As we have already shown in a previous publication [2], the multiplication of defects is needed to switch from needle to bush lithium growth. It may be assumed that the SEI is active in the process of defect formation and multiplication. Different SEI compositions lead to differences in thickness, electrical resistance, mechanical properties (e.g. compliance or fracture toughness), interface energies and wetting characteristics with lithium. Therefore, the differing SEI composition can easily explain that different morphologies are observed for the two electrolytes in **Fig. 8.1** and **Fig. 8.2**. The listed parameters of the SEI will affect lithium insertion into the growing structure and local variations of these parameters on a growing structure will define sites of accelerated and retarded lithium insertion. For example, cracking and incorporation of parts of the SEI layer into the lithium crystal may create further crystalline defects. Such an incorporation of SEI into lithium at dendrite locations was already observed by microtomography.[97]

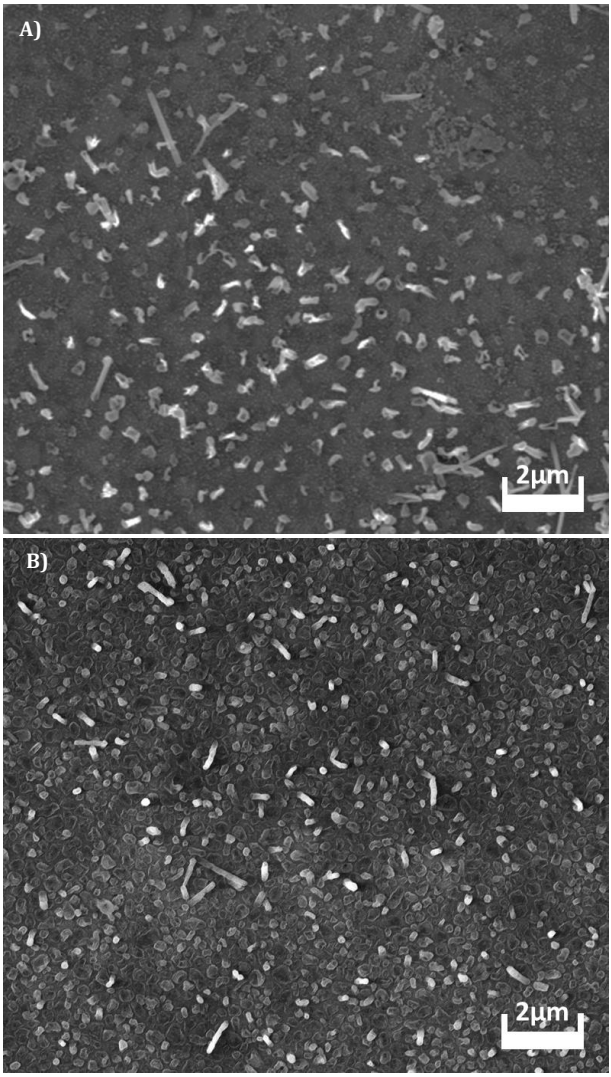

Fig. 8.3: SEM images of lithium needles grown on copper substrates at room temperature. Image A) shows needles grown electrochemically in LP30 electrolyte; image B) shows needles grown by PVD in vacuum.

In summary, we elucidated the mechanisms behind one-dimensional, needle growth and the three-dimensional, bush growth. The concepts presented are of general nature and not only specific to lithium so that it is plausible that they are also valid for the RT electrodeposition of materials with similar melting points. These include the metals sodium and tin that are also relevant for electrochemical energy storage. Our results show that on the one hand, needle growth turned out to be an inherent tendency of the metal. It combines a high atomic mobility caused by the low melting point with the insertion at defect sites, in particular, at the substrate-lithium interface. Hence, this mechanism is not depending on the deposition technique or the presence of a surface/interface layer. On the other hand, bush growth and the resulting deposits were found to be a phenomenon controlled by the SEI. Consequently, the SEI is the major factor determining the morphology of the deposits. Both growth modes are superimposed during electrochemical deposition, with the needle growth being the precursor of bush growth.[2] Conventional approaches to avoid dendrites do not seem sufficient, since needle growth is an inherent property of lithium. Such approaches include variations of ionic transport conditions (e.g. charge rate), and SEI modifications (e.g. optimized mechanical properties). In order to attack the dendrite problem at its root, we suggest to additionally reduce the mobility of lithium atoms. Blocking lithium diffusion on the substrate including its SEI should prevent the formation of filaments which are the precursors of dendrites.

9 Summary

Lithium dendrite formation and growth not only cause safety concerns in today's lithium-ion batteries but also prevent the application of lithium anodes with their superior properties in rechargeable systems. As a phenomenon known for almost 50 years, it has led to the proposition of numerous remedies and growth mechanisms. However, none of these attempts has led to the successful commercialization of lithium metal anodes in rechargeable batteries.

Assessment of Literature

Electric field enhancement at a protrusion, for example, is a physical fact, but simplistically applying it to electrochemical cells ignores the principle of electroneutrality inside a binary electrolyte. The magnitude of this tip effect has not been discussed critically in the literature yet; but it can be questioned if it is relevant, since for typical electrochemical conditions, the influence of migration caused by electric fields is limited compared to transport by diffusion driven by a gradient in concentration: Despite the fact that the electrical field can reach values exceeding 1000 V/m for large currents over long distances [128], it was shown that the transport due to the electric field can at maximum be as large as that due to concentration gradients [129]. For small currents, the electric field is confined to the electrochemical double layer (a few nm) and hardly extends into the electrolyte. Even if a field effect exists, it is questionable whether there is a "self-amplification" by a growing protrusion as suggested in [57] (independent of the concentration gradient effects discussed above), since the length of the growing protrusions (often >1 µm) might exceed the length scales of the electrochemical double layer where local electric fields can have significant impact.

Chazalviel's model based on the ionic concentration gradient could correctly predict the growth speed of dendrites as being proportional to the anion drift velocity. However, this model could not predict the onset of dendritic growth for current densities below the limiting current, which was explained by inhomogeneities that can result in locally higher current densities. Similar to electric field enhancement and spherical diffusion, this mechanism is not able to explain the observed growth at the base of a needle or bush [25, 62]. The mechanism proposed by Cohen et al. of SEI cracking gives a plausible explanation for dendrite growth initiation in an electrolyte but cannot explain why lithium needles form at all or why they were observed to grow from the base. Whisker-like extrusion was the only presented mechanism that could explain growth from the base of a needle, but failed to explain the reported elongation by aggregation at the tip of a needle. In addition, the pressure build-up inside the lithium surface is not viable for deposition experiments on substrates other than lithium. In this case, needles form directly on the substrate, without the necessary lithium volume the needle can extrude from.

Summary of Results

This thesis presents new observations with high spatial resolution of dendrite growth starting at the early stage of individual needles up to the behavior of large lithium bushes. The results contradict the existing theories of lithium dendrite growth. They show that largely investigated and discussed factors like current densities, ionic concentrations, whisker-forming stresses and SEI composition do not govern the onset of dendrite formation. The growth locations of a dendrite are a topic that is controversially discussed in the literature, and the proposed models are divided into two groups: those predicting tip growth and those predicting base growth. Hence, we studied the growth of lithium dendrites in a

commercial electrolyte by *in situ* light microscopy. Our optimized cell design and microscope setup enabled us to obtain *in situ* footage with unmatched resolution. This led to identification of the growth locations of lithium needles in two different commercial electrolytes for the first time and helped us to elucidate the relationship between lithium needles and bushes. SEM studies gave indications on the observed facets of lithium particles and the crystalline growth direction of needles. EBSD analysis revealed an influence of the copper substrate grain orientation and helped to identify the grain orientations that were more densely populated by deposits. Finally, we were able to grow lithium dendrites by thermal evaporation on a variety of substrates.

Fig. 9.1 shows a schematic that graphically summarizes our findings. (a) We found strong indication of the crystallinity of electrodeposited lithium: Lithium particles tend to form {110} facets, while we found strong indications for a <111> growth direction of needles. Our *in situ* data of needle growth showed that needle-like dendrites can grow by simultaneous atom insertion at the base, at the tip and at kinks. The presented theories only predict either growth at the tip or at the base, but not both simultaneously. In addition, growth at kinks was never observed before and is not predicted by any model. The EBSD analysis revealed that copper {111} surfaces are preferentially populated by lithium deposits. This emphasizes the importance of the lithium substrate interface and suggests that the lattice mismatch causes lattice distortion in the deposited lithium at the substrate interface. (b) These imperfections in the lattice are expected to control the nucleation and growth, not only at the base, but also at kinks with their high angle grain boundaries and at imperfections or non-active particles at the tip of the needles.

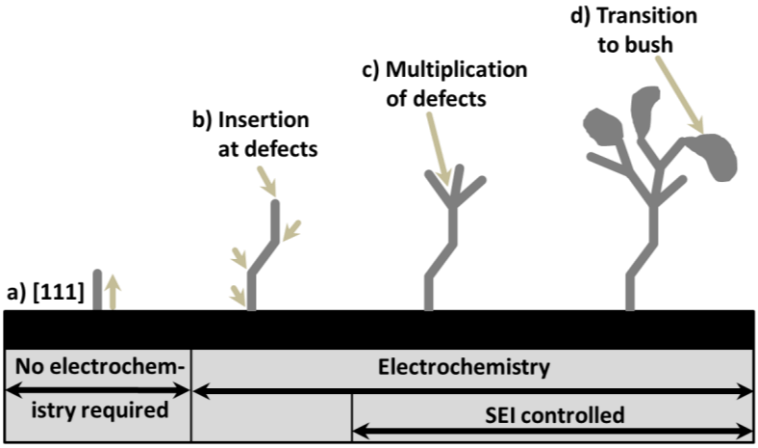

Fig. 9.1: Schematic describing of our results on electrochemical needle and bush growth.

The mechanism of atom insertion at crystalline defect sites – indicated by the growth of needles at interfaces and the influence of the orientation of the substrate crystal – does not rely on an electrochemical process. Consequently it was not only possible to grow lithium needles in different electrolytes, but also by physical vapor deposition in vacuum using similar deposition rates. This was never reported for lithium metal but in the terms of PVD this behavior is no exception to other metals. Nanowhisker growth of various materials by PVD was already reported. For most of these deposited materials a discontinuous dewetting layer (e.g. carbon) on the substrate is needed, in addition to a substrate temperature of about 65 % of the melting temperature of the deposited material. In the case of lithium, no surface layer was needed to form needles, and due to the low melting point of lithium, room temperature is already ca. 65 % of the melting temperature. Both conditions, the dewetting layer and the high substrate temperature, result in a high mobility of adatoms which is needed to

create the strong localization of deposition. High adatom mobility is also expected for electrochemical deposition. In addition, the dependence on the crystal orientation of the substrate was observed for electrodeposition in all electrolytes and after PVD of lithium, further supporting the view of a common insertion mechanism for both needle growth in electrochemical as well as vapor deposition.

Bush- or moss-like lithium dendrites are the most commonly observed form of lithium dendrites. (c) Our *in situ* images of the broadening and branching of a lithium needle in addition to the needles that were found at the basis of a bush-like structure suggest that needles are the precursor of bush-like dendrites. (d) In order to form a bush from a needle, a transition in the growth mode is necessary. The number of atom insertion sites is increasing; and the growth direction is no longer alongside the needle. In order to create more insertion sites, the crystalline defects need to multiply. However, the cause for the defect multiplication must be a process associated with the electrochemical process, as no bushes were observed in PVD. The comparison of dendrite formation in two different electrolytes showed that the morphology of bushes most likely is strongly affected by the SEI composition. This suggests that the SEI is not only controlling the growth of bushes but also is the cause of bush-like growth. In other words, the SEI seems to be responsible for the defect multiplication which results in the transition of the growth mode from needle to bush growth.

Bush growth showed to be particularly detrimental for the cycling efficiency and safety of a cell. During dissolution cycles, large proportions of bushes could not be dissolved as they were electrically isolated from the substrate. This was by the dissolution of the basis of the bush before the upper parts could be dissolved leading to large capacity losses. The remaining bush structure

stays attached to the surface by its SEI and acted as a nucleation point in the next deposition cycle; a new bush forms underneath pushing the remaining bush towards the counter electrode. This "push-remnant" mechanism makes bushes grow larger and larger during cycling which strongly increases the danger of a short circuit.

Outlook

According to the view established in this thesis, it is not surprising that so far countermeasures against dendrites have not proven successful since the roots of dendrite formation clearly lie outside of electrochemistry. In order to suppress lithium dendrite formation, the formation of lithium needles needs to be prevented. This means that either the surface energy of the substrate must be completely homogenous, or the adatom mobility must be reduced. While the former appears to be an impossible task, there are possible ways to reduce the adatom mobility. One possibility would be to reduce the temperature of the substrate during deposition of lithium well below 65 % of its melting temperature. In practice this would mean that a lithium metal battery needs to be cooled to temperatures below 0 °C during charging which raises many additional problems.[7] Another possibility would be to find an electrolyte additive (surfactant) that adsorbs on the substrate surface without being incorporated into the deposit; this could hinder the motion of lithium adatoms on the surface.

[7] It should be noted that such a cooling would probably not be helpful for the case of graphite electrodes due to the accompanying reduction of lithium diffusion in the graphite.

Bibliography

1. Steiger, J., D. Kramer, and R. Mönig, *Mechanisms of dendritic growth investigated by in situ light microscopy during electrodeposition and dissolution of lithium.* Journal of Power Sources, 2014. **261**: p. 112-119.
2. Steiger, J., D. Kramer, and R. Mönig, *Microscopic observations of the formation, growth and shrinkage of lithium moss during electrodeposition and dissolution.* Electrochimica Acta, 2014.
3. Steiger, J., et al., *Comparison of the Growth of Lithium Filaments and Dendrites Under Different Conditions.* accepted at Electrochemistry Communications, 2014.
4. Yamaki, J.I. and S.I. Tobishima, *Rechargeable lithium anodes.* Handbook of Battery Materials, Second Edition, 2011: p. 377-404.
5. Xu, W., et al., *Lithium metal anodes for rechargeable batteries.* Energy & Environmental Science, 2014. **7**(2): p. 513-537.
6. Richter, G., et al., *Ultrahigh Strength Single Crystalline Nanowhiskers Grown by Physical Vapor Deposition.* Nano Letters, 2009. **9**(8): p. 3048-3052.
7. Tarascon, J.M. and M. Armand, *Issues and challenges facing rechargeable lithium batteries.* Nature, 2001. **414**(6861): p. 359-367.
8. Kurzweil, P. and K. Brandt, *SECONDARY BATTERIES – LITHIUM RECHARGEABLE SYSTEMS | Overview*, in *Encyclopedia of Electrochemical Power Sources*, J. Garche, Editor 2009, Elsevier: Amsterdam. p. 1-26.
9. *Sion Power*. [cited September 15, 2014]; Available from: http://www.sionpower.com/index.html.
10. Brandt, K., *Historical development of secondary lithium batteries.* Solid State Ionics, 1994. **69**(3–4): p. 173-183.
11. Dahn, J., *Phase diagram of Li x C 6.* Physical Review B, 1991. **44**(17): p. 9170.

12. BBC. *Cause of battery fire identified in Cambridge study*. 2010 [cited September 15th, 2014]; Available from: http://news.bbc.co.uk/2/hi/uk_news/england/cambridgeshire/8687963.stm.
13. Ostrower, J. and A. Pasztor. *Microscopic 'Dendrites' a Focus in Boeing Dreamliner Probe*. 2013 [cited September 15, 2014]; Available from: http://online.wsj.com/news/articles/SB10001424127887324880504578298673566960476.
14. Bresser, D., S. Passerini, and B. Scrosati, *Recent progress and remaining challenges in sulfur-based lithium secondary batteries–a review.* Chem. Commun., 2013. **49**(90): p. 10545-10562.
15. Whittingham, M.S., *History, evolution, and future status of energy storage.* Proceedings of the IEEE, 2012. **100**(Special Centennial Issue): p. 1518-1534.
16. Barton, J.L. and J.O.M. Bockris, *The Electrolytic Growth of Dendrites from Ionic Solutions.* Proceedings of the Royal Society of London. Series A. Mathematical and Physical Sciences, 1962. **268**(1335): p. 485-505.
17. Despić, A. and K.I. Popov, *Transport-controlled deposition and dissolution of metals*, in *Modern Aspects of Electrochemistry No. 7*1972, Springer. p. 199-313.
18. Despić, A.R. and K.I. Popov, *Transport-Controlled Deposition and Dissolution of Metals*, in *Modern Aspects of Electrochemistry No. 7*, B.E. Conway and J.O.M. Bockris, Editors. 1972, Springer US. p. 199-313.
19. Fleury, V., et al., *The role of the anions in the growth speed of fractal electrodeposits.* Journal of Electroanalytical Chemistry and Interfacial Electrochemistry, 1990. **290**(1): p. 249-255.
20. Chazalviel, J.N., *Electrochemical aspects of the generation of ramified metallic electrodeposits.* Physical Review A, 1990. **42**(12): p. 7355-7367.
21. Brissot, C., et al., *In situ study of dendritic growth inlithium/PEO-salt/lithium cells.* Electrochimica Acta, 1998. **43**(10–11): p. 1569-1574.

22. Brissot, C., et al., *Dendritic growth mechanisms in lithium/ polymer cells.* Journal of Power Sources, 1999. **81**: p. 925-929.
23. Rosso, M., et al., *Onset of dendritic growth in lithium/polymer cells.* Journal of Power Sources, 2001. **97–98**(0): p. 804-806.
24. Rosso, M., J.N. Chazalviel, and E. Chassaing, *Calculation of the space charge in electrodeposition from a binary electrolyte.* Journal of Electroanalytical Chemistry, 2006. **587**(2): p. 323-328.
25. Crowther, O. and A.C. West, *Effect of Electrolyte Composition on Lithium Dendrite Growth.* Journal of The Electrochemical Society, 2008. **155**(11): p. A806-A811.
26. Orsini, F., et al., *In situ scanning electron microscopy (SEM) observation of interfaces within plastic lithium batteries.* Journal of Power Sources, 1998. **76**(1): p. 19-29.
27. Orsini, F., et al., *In situ SEM study of the interfaces in plastic lithium cells.* Journal of Power Sources, 1999. **81**: p. 918-921.
28. Dollé, M., et al., *Live scanning electron microscope observations of dendritic growth in lithium/polymer cells.* Electrochemical and solid-state letters, 2002. **5**(12): p. A286-A289.
29. Jorne, J., Y.J. Lii, and K.E. Yee, *Suppression of Dendrites and Roughness during Electrodeposition by Impinging Flow.* Journal of The Electrochemical Society, 1987. **134**(6): p. 1399-1402.
30. Yang, X., et al., *Electrodeposition of lithium film under dynamic conditions and its application in all-solid-state rechargeable lithium battery.* Solid State Ionics, 2005. **176**(11–12): p. 1051-1055.
31. Mayers, M.Z., J.W. Kaminski, and T.F. Miller III, *Suppression of dendrite formation via pulse charging in rechargeable lithium metal batteries.* The Journal of Physical Chemistry C, 2012. **116**(50): p. 26214-26221.
32. Suo, L., et al., *A new class of solvent-in-salt electrolyte for high-energy rechargeable metallic lithium batteries.* Nature Communications, 2013. **4**: p. 1481.

33. Peled, E., et al., *Composition, depth profiles and lateral distribution of materials in the SEI built on HOPG-TOF SIMS and XPS studies.* Journal of Power Sources, 2001. **97–98**(0): p. 52-57.
34. Peled, E. and D. Golodnitsky, *. SEI on lithium, graphite, disordered carbons and tin-based alloys.*
35. Aurbach, D. and A. Zaban, *Impedance spectroscope of lithium electrodes: Part 2. The behaviour in propylene carbonate solutions — the significance of the data obtained.* Journal of Electroanalytical Chemistry, 1994. **367**(1–2): p. 15-25.
36. Cohen, Y.S., Y. Cohen, and D. Aurbach, *Micromorphological Studies of Lithium Electrodes in Alkyl Carbonate Solutions Using in Situ Atomic Force Microscopy.* The Journal of Physical Chemistry B, 2000. **104**(51): p. 12282-12291.
37. Aurbach, D. and Y. Cohen, *The application of atomic force microscopy for the study of li deposition processes.* Journal of The Electrochemical Society, 1996. **143**(11): p. 3525-3532.
38. Aurbach, D., et al., *The behaviour of lithium electrodes in propylene and ethylene carbonate: The major factors that influence Li cycling efficiency.* Journal of Electroanalytical Chemistry, 1992. **339**(1): p. 451-471.
39. Aurbach, D. and Y. Cohen, *Morphological studies of Li deposition processes in $LiAsF_6$/PC solutions by in situ atomic force microscopy.* Journal of The Electrochemical Society, 1997. **144**(10): p. 3355-3360.
40. Naoi, K., et al., *The Surface Film Formed on a Lithium Metal Electrode in a New Imide Electrolyte, Lithium Bis (perfluoroethylsulfonylimide)[$LiN(C_2F_5SO_2)_2$].* Journal of The Electrochemical Society, 1999. **146**(2): p. 462-469.
41. Hayashi, K., et al., *Mixed solvent electrolyte for high voltage lithium metal secondary cells.* Electrochimica Acta, 1999. **44**(14): p. 2337-2344.
42. Aurbach, D., et al., *The electrochemical behaviour of 1, 3-dioxolane—$LiClO_4$ solutions—I. Uncontaminated solutions.* Electrochimica Acta, 1990. **35**(3): p. 625-638.
43. Aurbach, D., *Review of selected electrode–solution interactions which determine the performance of Li and Li*

ion batteries. Journal of Power Sources, 2000. **89**(2): p. 206-218.
44. Takehara, Z.-i., *Future prospects of the lithium metal anode.* Journal of Power Sources, 1997. **68**(1): p. 82-86.
45. Shiraishi, S., K. Kanamura, and Z.i. Takehara, *Surface Condition Changes in Lithium Metal Deposited in Nonaqueous Electrolyte Containing HF by Dissolution-Deposition Cycles.* Journal of The Electrochemical Society, 1999. **146**(5): p. 1633-1639.
46. Mogi, R., et al., *Effects of some organic additives on lithium deposition in propylene carbonate.* Journal of The Electrochemical Society, 2002. **149**(12): p. A1578-A1583.
47. Ota, H., et al., *Effect of vinylene carbonate as additive to electrolyte for lithium metal anode.* Electrochimica Acta, 2004. **49**(4): p. 565-572.
48. Ishikawa, M., M. Morita, and Y. Matsuda, *In situ scanning vibrating electrode technique for lithium metal anodes.* Journal of Power Sources, 1997. **68**(2): p. 501-505.
49. Matsuda, Y., *Behavior of lithium/electrolyte interface in organic solutions.* Journal of Power Sources, 1993. **43**(1): p. 1-7.
50. Ishikawa, M., et al., *In situ scanning vibrating electrode technique for the characterization of interface between lithium electrode and electrolytes containing additives.* Journal of The Electrochemical Society, 1994. **141**(12): p. L159-L161.
51. Yoon, S., et al., *Enhanced cyclability and surface characteristics of lithium batteries by Li–Mg co-deposition and addition of HF acid in electrolyte.* Electrochimica Acta, 2008. **53**(5): p. 2501-2506.
52. Stark, J.K., Y. Ding, and P.A. Kohl, *Dendrite-Free Electrodeposition and Reoxidation of Lithium-Sodium Alloy for Metal-Anode Battery.* Journal of The Electrochemical Society, 2011. **158**(10): p. A1100-A1105.
53. Vega, J.A., J. Zhou, and P.A. Kohl, *Electrochemical comparison and deposition of lithium and potassium from phosphonium-and ammonium-TFSI ionic liquids.* Journal of The Electrochemical Society, 2009. **156**(4): p. A253-A259.

54. Monroe, C. and J. Newman, *Dendrite Growth in Lithium/ Polymer Systems: A Propagation Model for Liquid Electrolytes under Galvanostatic Conditions.* Journal of The Electrochemical Society, 2003. **150**(10): p. A1377-A1384.
55. Akolkar, R., *Modeling dendrite growth during lithium electrodeposition at sub-ambient temperature.* Journal of Power Sources, 2014. **246**(0): p. 84-89.
56. Chianelli, R.R., *Microscopic studies of transition metal chalcogenides.* Journal of Crystal Growth, 1976. **34**(2): p. 239-244.
57. Ding, F., et al., *Dendrite-Free Lithium Deposition via Self-Healing Electrostatic Shield Mechanism.* Journal of the American Chemical Society, 2013. **135**(11): p. 4450-4456.
58. Ding, F., et al., *Effects of Cesium Cations in Lithium Deposition via Self-Healing Electrostatic Shield Mechanism.* The Journal of Physical Chemistry C, 2014. **118**(8): p. 4043-4049.
59. Halpin-Healy, T. and Y.-C. Zhang, *Kinetic roughening phenomena, stochastic growth, directed polymers and all that. Aspects of multidisciplinary statistical mechanics.* Physics Reports, 1995. **254**(4–6): p. 215-414.
60. Matteo, N., C. Mario, and C. Rodolfo, *Kinetic roughening in a realistic model of non-conserved interface growth.* Journal of Statistical Mechanics: Theory and Experiment, 2009. **2009**(02): p. P02036.
61. Nicoli, M., M. Castro, and R. Cuerno, *Unified moving-boundary model with fluctuations for unstable diffusive growth.* Physical Review E, 2008. **78**(2): p. 021601.
62. Yamaki, J.-i., et al., *A consideration of the morphology of electrochemically deposited lithium in an organic electrolyte.* Journal of Power Sources, 1998. **74**(2): p. 219-227.
63. Yamaki, J.-I. and S.-I. Tobishima, *Rechargeable Lithium Anodes*, in *Handbook of Battery Materials*2011, Wiley-VCH Verlag GmbH & Co. KGaA. p. 377-404.
64. Zhang, X.-W., et al., *Inhibition of lithium dendrites by fumed silica-based composite electrolytes.* Journal of The Electrochemical Society, 2004. **151**(8): p. A1257-A1263.

65. Tatsuma, T., M. Taguchi, and N. Oyama, *Inhibition effect of covalently cross-linked gel electrolytes on lithium dendrite formation.* Electrochimica Acta, 2001. **46**(8): p. 1201-1205.
66. Armand, M., M. Duclot, and P. Rigaud, *Polymer solid electrolytes: Stability domain.* Solid State Ionics, 1981. **3**: p. 429-430.
67. Scrosati, B., *Electrode kinetics in polymer electrolyte solid-state cells.* British polymer journal, 1988. **20**(3): p. 219-226.
68. Hirai, T., I. Yoshimatsu, and J.i. Yamaki, *Influence of Electrolyte on Lithium Cycling Efficiency with Pressurized Electrode Stack.* Journal of The Electrochemical Society, 1994. **141**(3): p. 611-614.
69. Gireaud, L., et al., *Lithium metal stripping/plating mechanisms studies: A metallurgical approach.* Electrochemistry Communications, 2006. **8**(10): p. 1639-1649.
70. Park, H.E., C.H. Hong, and W.Y. Yoon, *The effect of internal resistance on dendritic growth on lithium metal electrodes in the lithium secondary batteries.* Journal of Power Sources, 2008. **178**(2): p. 765-768.
71. Mogi, R., et al., *In situ atomic force microscopy observation of lithium deposition at an elevated temperature.* Journal of Power Sources, 2001. **97–98**(0): p. 265-268.
72. Li, Z., et al., *A review of lithium deposition in lithium-ion and lithium metal secondary batteries.* Journal of Power Sources, 2014. **254**(0): p. 168-182.
73. Chason, E., et al., *Growth of whiskers from Sn surfaces: Driving forces and growth mechanisms.* Progress in Surface Science, 2013. **88**(2): p. 103-131.
74. Galyon, G.T., *Annotated tin whisker bibliography and anthology.* IEEE Transactions on Electronics Packaging Manufacturing, 2005. **28**(1): p. 94-122.
75. Walker, E., *Whisker Growth on Silver Tipped Contacts. Report on investigation of an electrical accident at Coking plant in 1979.* UK Health and Safety Executive (HSE), UK British Standard Institute (BSI), 1999.

76. Teverovsky, A., *Gold Whiskers: Introducing a New Member to the Family*, in *Internal Memorandum-NASA Goddard Space Flight Center*2003, QSS Group Inc./Goddard Operations.
77. Turner, T. and R. Parsons, *A new failure mechanism: Al-Si bond pad whisker growth during life test.* Components, Hybrids, and Manufacturing Technology, IEEE Transactions on, 1982. **5**(4): p. 431-435.
78. Sines, G., *Filamentary Crystals grown from the Solid Metal.* Journal of the Physical Society of Japan, 1960. **15**(7): p. 1199-1210.
79. Wang, Z.M., ed. *One-Dimensional Nanostructures*. Lecture Notes in Nanoscale Science and Technology, ed. Z.M.W. Wang, Andreas; Salamo, Gregory; Kishimoto, Naoki;2008, Springer Science+Business Media, LLC.
80. Choi, H.-J., *Vapor–Liquid–Solid Growth of Semiconductor Nanowires*, in *Semiconductor Nanostructures for Optoelectronic Devices*2012, Springer. p. 1-36.
81. Lee, S., et al., *Oxide-assisted semiconductor nanowire growth.* MRS bulletin, 1999. **24**(08): p. 36-42.
82. Schamel, M., et al., *The filamentary growth of metals.* International Journal of Materials Research, 2011. **102**(7): p. 828-836.
83. Ruth, V. and J. Hirth, *Kinetics of Diffusion-Controlled Whisker Growth.* The Journal of Chemical Physics, 1964. **41**(10): p. 3139-3149.
84. Aurbach, D., et al., *Attempts to Improve the Behavior of Li Electrodes in Rechargeable Lithium Batteries.* Journal of The Electrochemical Society, 2002. **149**(10): p. A1267-A1277.
85. Herstedt, M., et al., *Electrolyte additives for enhanced thermal stability of the graphite anode interface in a Li-ion battery.* Electrochimica Acta, 2004. **49**(14): p. 2351-2359.
86. Zhang, S.S., *Liquid electrolyte lithium/sulfur battery: fundamental chemistry, problems, and solutions.* Journal of Power Sources, 2013. **231**: p. 153-162.
87. Gao, J., et al., *Effects of liquid electrolytes on the charge–discharge performance of rechargeable lithium/sulfur batteries: electrochemical and in-situ X-ray absorption*

spectroscopic studies. The Journal of Physical Chemistry C, 2011. **115**(50): p. 25132-25137.
88. Deegan, R.D., et al., *Capillary flow as the cause of ring stains from dried liquid drops.* Nature, 1997. **389**(6653): p. 827-829.
89. Hu, H. and R.G. Larson, *Marangoni Effect Reverses Coffee-Ring Depositions.* The Journal of Physical Chemistry B, 2006. **110**(14): p. 7090-7094.
90. Zucker, R.V., et al., *New software tools for the calculation and display of isolated and attached interfacial-energy minimizing particle shapes.* Journal of Materials Science, 2012. **47**(24): p. 8290-8302.
91. Jäckle, M. and A. Groß, *Comparison of lithium, sodium and magnesium battery anode materials on a microscopic level using DFT.* submitted to Phys. Rev. B, 2014(DOI: 10.1063/1.4901055).
92. İnoğlu, N. and J.R. Kitchin, *Atomistic thermodynamics study of the adsorption and the effects of water–gas shift reactants on Cu catalysts under reaction conditions.* Journal of Catalysis, 2009. **261**(2): p. 188-194.
93. Langenhuizen, N., *The effect of mass transport on Li deposition and dissolution.* Journal of The Electrochemical Society, 1998. **145**(9): p. 3094-3099.
94. Nishida, T., et al., *Optical observation of Li dendrite growth in ionic liquid.* Electrochimica Acta, 2013. **100**(0): p. 333-341.
95. Sagane, F., et al., *Effects of current densities on the lithium plating morphology at a lithium phosphorus oxynitride glass electrolyte/copper thin film interface.* Journal of Power Sources, 2013. **233**(0): p. 34-42.
96. Andersson, A.M. and K. Edström, *Chemical Composition and Morphology of the Elevated Temperature SEI on Graphite.* Journal of The Electrochemical Society, 2001. **148**(10): p. A1100-A1109.
97. Harry, K.J., et al., *Detection of subsurface structures underneath dendrites formed on cycled lithium metal electrodes.* Nature Materials, 2014. **13**(1): p. 69-73.
98. Kanamura, K., et al., *X-Ray Photoelectron Spectroscopic Analysis and Scanning Electron Microscopic Observation of*

the Lithium Surface Immersed in Nonaqueous Solvents. Journal of The Electrochemical Society, 1994. **141**(9): p. 2379-2385.

99. Witten, T.A. and L.M. Sander, *Diffusion-limited aggregation.* Physical Review B, 1983. **27**(9): p. 5686.
100. Wranglén, G., *Dendrites and growth layers in the electrocrystallization of metals.* Electrochimica Acta, 1960. **2**(1–3): p. 130-143.
101. Sobiech, M., et al., *Local, submicron, strain gradients as the cause of Sn whisker growth.* Applied Physics Letters, 2009. **94**(22): p. 221901-3.
102. Sobiech, M., et al., *Phase formation at the Sn/Cu interface during room temperature aging: Microstructural evolution, whiskering, and interface thermodynamics.* Journal of Materials Research, 2011. **26**(12): p. 1482-1493.
103. Stark, J.K., Y. Ding, and P.A. Kohl, *Nucleation of Electrodeposited Lithium Metal: Dendritic Growth and the Effect of Co-Deposited Sodium.* Journal of The Electrochemical Society, 2013. **160**(9): p. D337-D342.
104. Liu, X.H., et al., *Lithium fiber growth on the anode in a nanowire lithium ion battery during charging.* Applied Physics Letters, 2011. **98**(18): p. 183107-3.
105. Verma, P., P. Maire, and P. Novák, *A review of the features and analyses of the solid electrolyte interphase in Li-ion batteries.* Electrochimica Acta, 2010. **55**(22): p. 6332-6341.
106. Nishikawa, K., et al., *In Situ Observation of Dendrite Growth of Electrodeposited Li Metal.* Journal of The Electrochemical Society, 2010. **157**(11): p. A1212-A1217.
107. Shipman, J.T.W., Jerry D.; Higgins, Charles A., *An Introduction to Physical Science*. 13th Edition ed2013: Brooks/Cole, Cengage Learning.
108. Nishikawa, K., et al., *Li dendrite growth and Li+ ionic mass transfer phenomenon.* Journal of Electroanalytical Chemistry, 2011. **661**(1): p. 84-89.
109. Ghassemi, H., et al., *Real-time observation of lithium fibers growth inside a nanoscale lithium-ion battery.* Applied Physics Letters, 2011. **99**(12): p. 123113.

110. Arakawa, M., et al., *Lithium electrode cycleability and morphology dependence on current density.* Journal of Power Sources, 1993. **43**(1): p. 27-35.
111. Meakin, P., *Formation of fractal clusters and networks by irreversible diffusion-limited aggregation.* Physical Review Letters, 1983. **51**(13): p. 1119.
112. Selim, R. and P. Bro, *Some Observations on Rechargeable Lithium Electrodes in a Propylene Carbonate Electrolyte.* Journal of The Electrochemical Society, 1974. **121**(11): p. 1457-1459.
113. Peled, E., *The electrochemical behavior of alkali and alkaline earth metals in nonaqueous battery systems—the solid electrolyte interphase model.* Journal of The Electrochemical Society, 1979. **126**(12): p. 2047-2051.
114. Yoshimatsu, I., T. Hirai, and J.i. Yamaki, *Lithium electrode morphology during cycling in lithium cells.* Journal of The Electrochemical Society, 1988. **135**(10): p. 2422-2427.
115. Bhattacharyya, A.J. and J. Maier, *Second Phase Effects on the Conductivity of Non-Aqueous Salt Solutions:"Soggy Sand Electrolytes".* Advanced Materials, 2004. **16**(9-10): p. 811-814.
116. Bhattacharyya, A.J., et al., *New class of soft matter electrolytes obtained via heterogeneous doping: Percolation effects in "soggy sand" electrolytes.* Solid State Ionics, 2006. **177**(26): p. 2565-2568.
117. Pfaffenhuber, C., et al., *Soggy-sand electrolytes: status and perspectives.* Physical Chemistry Chemical Physics, 2013. **15**(42): p. 18318-18335.
118. Pichl, W., *Recrystallization of partially transformed lithium single crystals.* physica status solidi (a), 1996. **158**(1): p. 101-106.
119. Aurbach, D. and A. Zaban, *Impedance Spectroscopy of Nonactive Metal Electrodes at Low Potentials in Propylene Carbonate Solutions A Comparison to Studies of Li Electrodes.* Journal of The Electrochemical Society, 1994. **141**(7): p. 1808-1819.
120. Barkey, D., F. Oberholtzer, and Q. Wu, *Kinetic Anisotropy and Dendritic Growth in Electrochemical Deposition.* Physical Review Letters, 1995. **75**(16): p. 2980-2983.

121. Oberholtzer, F., D. Barkey, and Q. Wu, *Kinetic selection of morphology and growth velocity in electrochemical deposition.* Physical Review E, 1998. **57**(6): p. 6955-6961.
122. BASF. *Selectilyte™ LP*. 2012 [cited 2014; Available from: http://www.catalysts.pro/downloads/public/pdfs/Battery%20Materials/52012BF-9822_US_SelectilyteLP_Datasheet-051512.pdf.
123. Aurbach, D., Y. Gofer, and J. Langzam, *The correlation between surface chemistry, surface morphology, and cycling efficiency of lithium electrodes in a few polar aprotic systems.* Journal of The Electrochemical Society, 1989. **136**(11): p. 3198-3205.
124. Aurbach, D., et al., *Correlation between surface chemistry, morphology, cycling efficiency and interfacial properties of Li electrodes in solutions containing different Li salts.* Electrochimica Acta, 1994. **39**(1): p. 51-71.
125. Sekerka, R.F., *Equilibrium and growth shapes of crystals: how do they differ and why should we care?* Crystal Research and Technology, 2005. **40**(4-5): p. 291-306.
126. Price, P., D. Vermilyea, and M. Webb, *On the growth and properties of electrolytic whiskers.* Acta Metallurgica, 1958. **6**(8): p. 524-531.
127. Popov, K., M. Pavlović, and M. Maksimović, *Comparison of the critical conditions for initiation of dendritic growth and powder formation in potentiostatic and galvanostatic copper electrodeposition.* Journal of Applied Electrochemistry, 1982. **12**(5): p. 525-531.
128. Rademaker, T., et al., *On the Deviation of Electro-Neutrality in Li-Ion Battery Electrolytes.* Journal of The Electrochemical Society, 2014. **161**(8): p. E3365-E3372.
129. Vetter, K.J., et al., *Electrochemical kinetics: theoretical aspects.* Academic Press, New York, 1967.

A Appendix

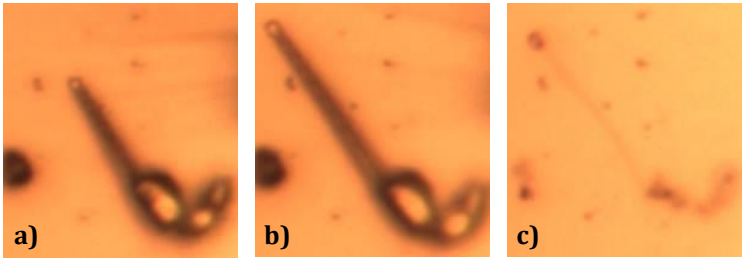

Fig. A 1**:** From a) to b), the needle grows in length, but the shape of the tip remains the same. c) After dissolution of the needle, this tip is still visible.

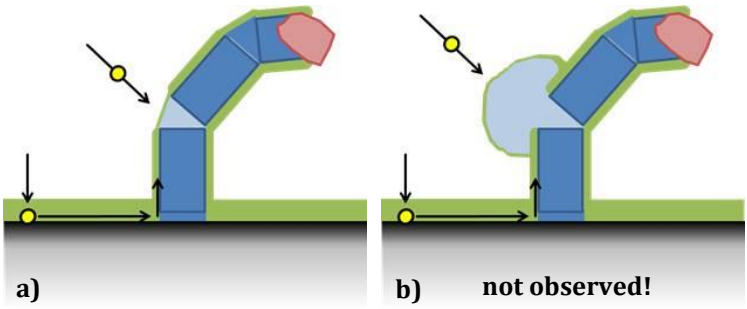

Fig. A 2: Schematic a) shows the plating process at a kink due to defects in the SEI. Schematic b) shows the resulting three dimensional plating if the insertion into defects in the crystal is neglected. Such a 3D deposition at kinks was not observed in the experiments, instead, elongation of the segments took place, as exemplified by **Fig. 5.4**

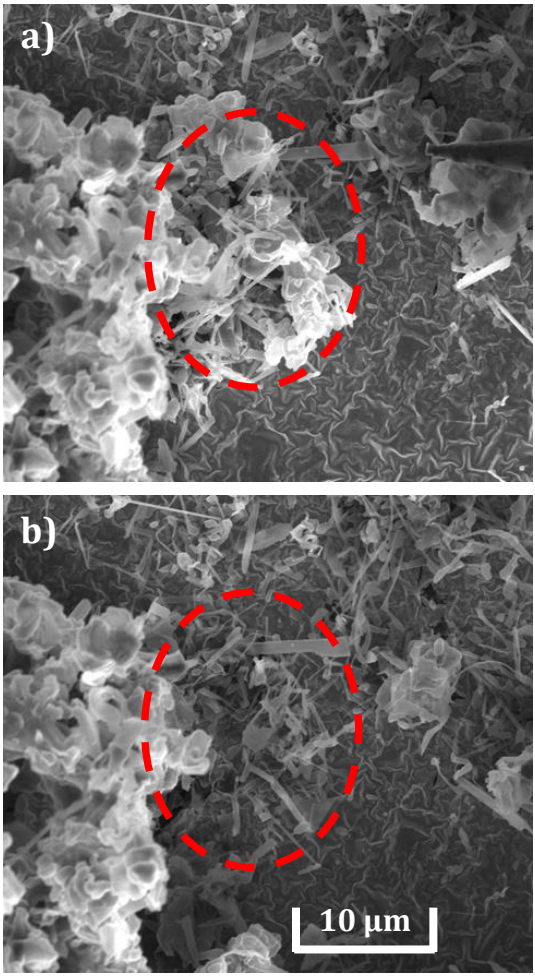

Fig. A 3: SEM images of bush-like dendrites grown on a tungsten substrate. A micromanipulator was used to remove the upper parts of a bush, and revealed a needle structure underneath.

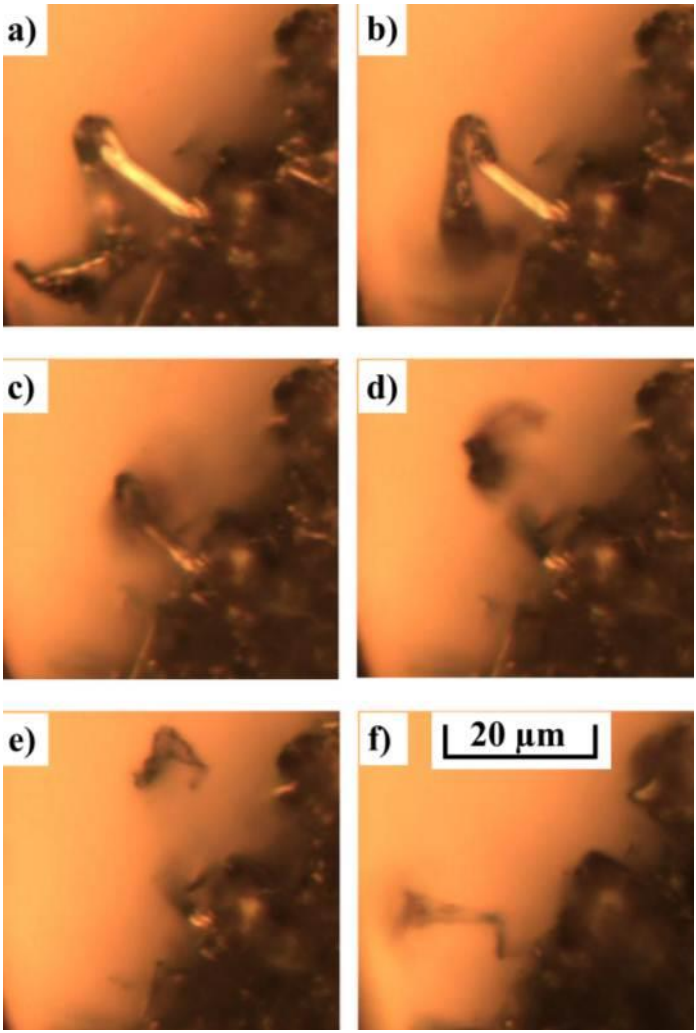

Fig. A 4: In *situ* light microscopy of the stripping of the bush-like structure on tungsten from Fig. 2. Dissolution starts from the tip a thin hollow shell remains. The images cover a time span of 20 minutes.

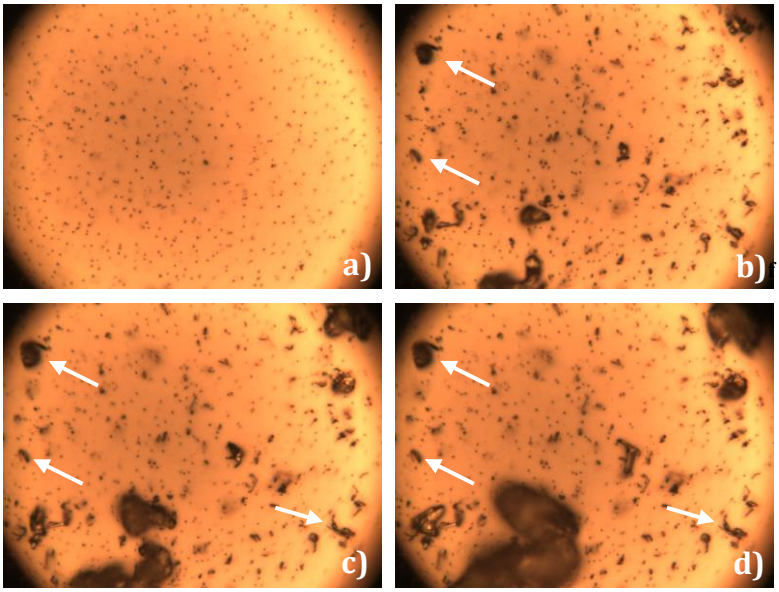

Fig. A 5: *In situ* light microscopy overview of a tungsten substrate during plating. The arrows mark structures that formed, but seized to grow. The images cover a time span of 45 minutes.

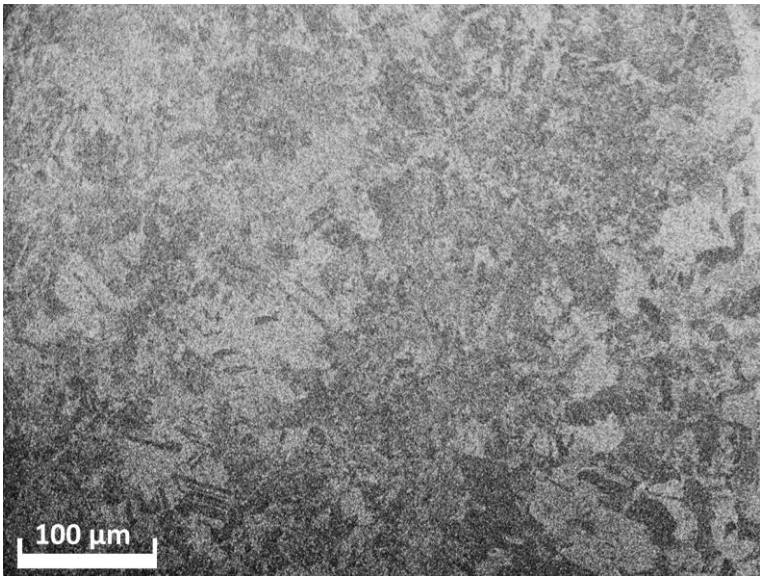

Fig. A 6: SEM image of lithium deposited by PVD onto a vibratory polished, oxide free copper substrate. The image was taken with the “in lens” detector. The amount of deposited lithium appears to be grain orientation selective.

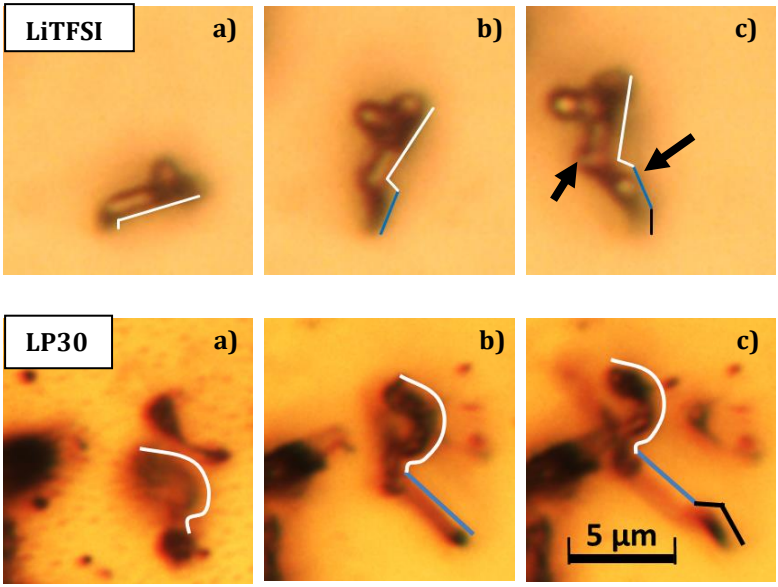

Fig. A 7: Growth of a lithium needle in LiTFSI (above) and LP30 (below). Atoms are inserted at the base. An initial structure shown in both images a) and marked in white. Images b) show the structures getting pushed upwards by needle-like deposition (blue) underneath it. Images c) show new segments (black) that were added to the base. The arrows mark spheres that were generated at the kinks of a filament in LiTFSI.

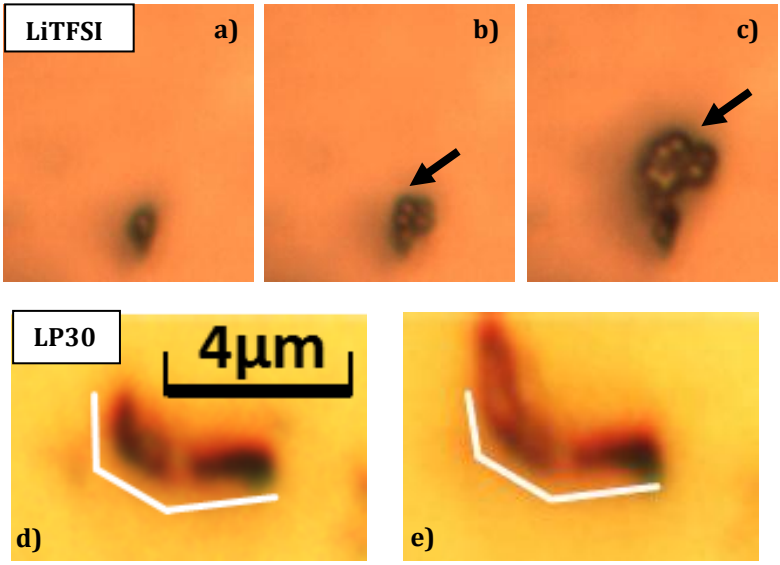

Fig. A 8: Light microscopy images of the growth of a lithium deposit in LiTFSI (above, a, b, c) and of a lithium needle in LP30 (below, d, e). Spheres are deposited at the tip area of the needle in LP30 while the structure gained in length by growth from the base.

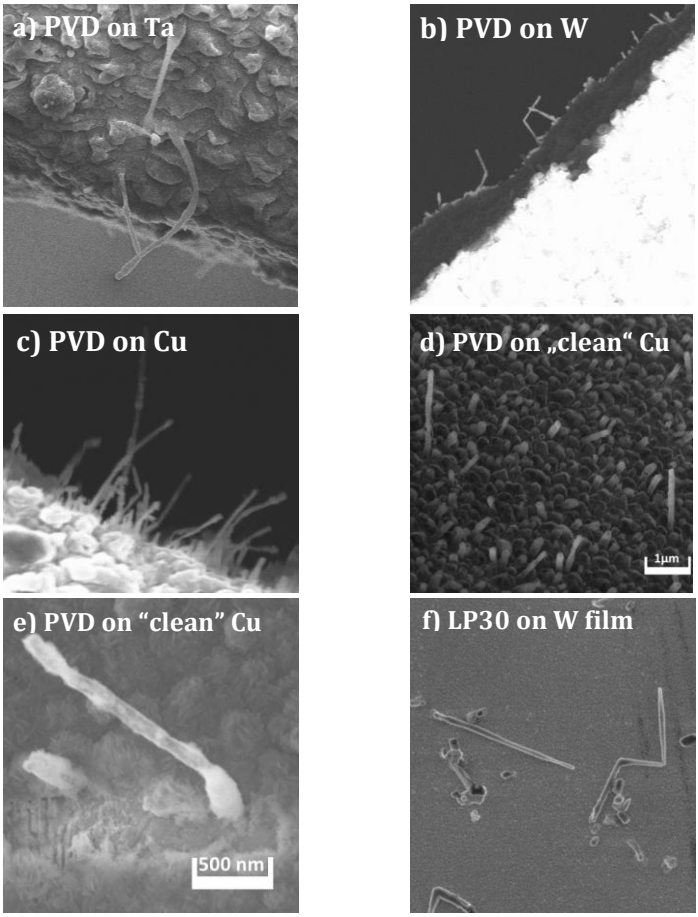

Fig. A 9: SEM images of lithium needles grown by PVD (images a to e) and electrodeposition (f). Deposits are grown by PVD on (a) tantalum (b) tungsten and (c) copper foil. d) shows Li needles grown on a vibratory polished and oxide free copper surface. e) shows a cross section of a needle base grown on the former surface. f) shows lithium needles grown on a copper surface by electrodeposition in LP30 electrolyte.